Seismic performance of precast concrete beam–column connections with innovative dry mechanical splice

Seon-Hoon Kim, Deuckhang "DK" Lee, Wei Zhang, and Jae-Hyun Kim

- The proposed self-sustaining dry precast concrete system uses mechanical splices to achieve self-stability during erection without temporary shoring. This reduces construction time and costs of multistory moment frames while maintaining compliance with special and intermediate seismic detailing requirements.
- Experimental testing confirmed flexural failure at intended beam locations consistent with strong column–weak beam principles; in the special precast concrete specimen, fractures occurred outside the splice region, validating that the dry mechanical splice does not govern the failure mechanism.
- Emulative seismic performance was comparable between the dry precast concrete and monolithic cast-in-place specimens, supporting the use of the proposed precast concrete system in high-seismic applications.
- A nonlinear model combining concentrated plastic hinges with an explicit joint rotational spring accurately captured cyclic response characteristics (stiffness degradation, pinching, and strength loss), providing a validated analytical framework for performance-based evaluation of precast concrete beam–column joint details.

The precast concrete industry is undergoing rapid transformation in response to climate change–driven hazards, ecofriendly construction practices aligned with carbon-neutrality goals, and rising construction labor costs associated with demographic shifts in the workforce. As a result, offsite construction—in which primary structural components are fabricated in a plant and transported to and assembled on-site—has gained prominence as a key project-delivery method. Off-site construction has improved construction efficiency and safety, and reduced environmental impacts, by reducing dependence on labor-intensive site operations.[1–5] In conventional construction of precast concrete moment frames, upper and lower columns are spliced using wet joints, where grout is injected into splice sleeves, which requires curing until it attains a target compressive strength. This common practice inevitably requires extensive temporary shoring and delays construction of upper stories, which increases project costs, thus diminishing the inherent advantages of precast concrete systems in terms of construction speed and constructibility.

Given these limitations, interest is growing in dry splice connections, which can eliminate on-site grouting and curing while providing reliable structural performance under gravity and seismic loading. **Figure 1** illustrates designs for using dry precast concrete beam–column connections in a logistics warehouse, aimed at recovering delays in the construction schedule. The precast concrete moment frame system was designed and constructed using fully dry mechanical connections in beam–column joints, providing im-

Precast concrete in large warehouse

Column splices

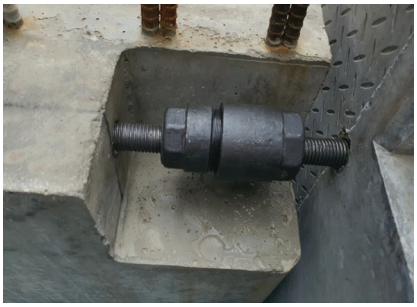

Beam-column splice

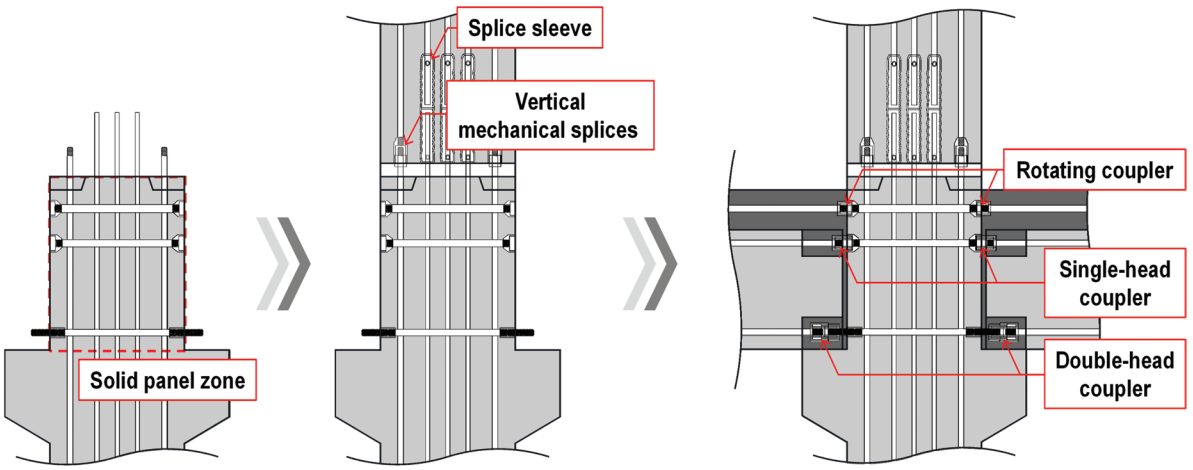

Solid panel zone in self-sustaining dry precast concrete system

Figure 1. Construction of dry precast concrete beam–column connections.

mediate structural stability under construction loads without the need for temporary supports.

A self-sustaining dry precast concrete system allows two or more stories of precast concrete columns with precast concrete beams to stand without shoring or temporary supports through dry mechanical splices in the vertical direction. This system minimizes dependence on curing and temporary supports, ensures immediate structural stability during erection, and maximizes cost-savings through significant reductions in construction time. Despite these advantages, implementing dry splicing remains limited in practice because of uncertainties regarding its structural performance, particularly seismic performance under cyclic loading, variability in quality control, and a lack of accumulated construction experience.[6–9]

Figure 2 compares the construction process of conventional and dry precast concrete moment frame systems. The conventional wet-splicing method requires multiple temporary supports to maintain column stability during erection. Moreover, once topping concrete is placed over the precast concrete floor slabs, construction of the upper stories must be suspended to allow the concrete to cure, limiting potential schedule gains.

As Fig. 2 shows, dry mechanical splices in precast concrete columns can support three or more stories of columns without temporary shoring. During erection, gravity loads are primarily carried by the corbel/beam seat and the prefabricated solid panel zone, while continuity across the joint is secured by the dry mechanical splices. This rapid-erection sequence substantially reduces both construction time and associated costs.[10–11]

In this study, researchers used structural testing to evaluate precast concrete special and intermediate moment frames with innovative dry mechanical splices capable of transmitting both compression and tension. The study verified the emulative seismic performance of the dry splices by comparing them with the performance of monolithic specimens. In addition, the researchers developed a nonlinear model and confirmed its applicability based on experimental results.

Experimental program

New dry-splicing system

Figure 3 presents details of the dry mechanical splices proposed in this study, which include:

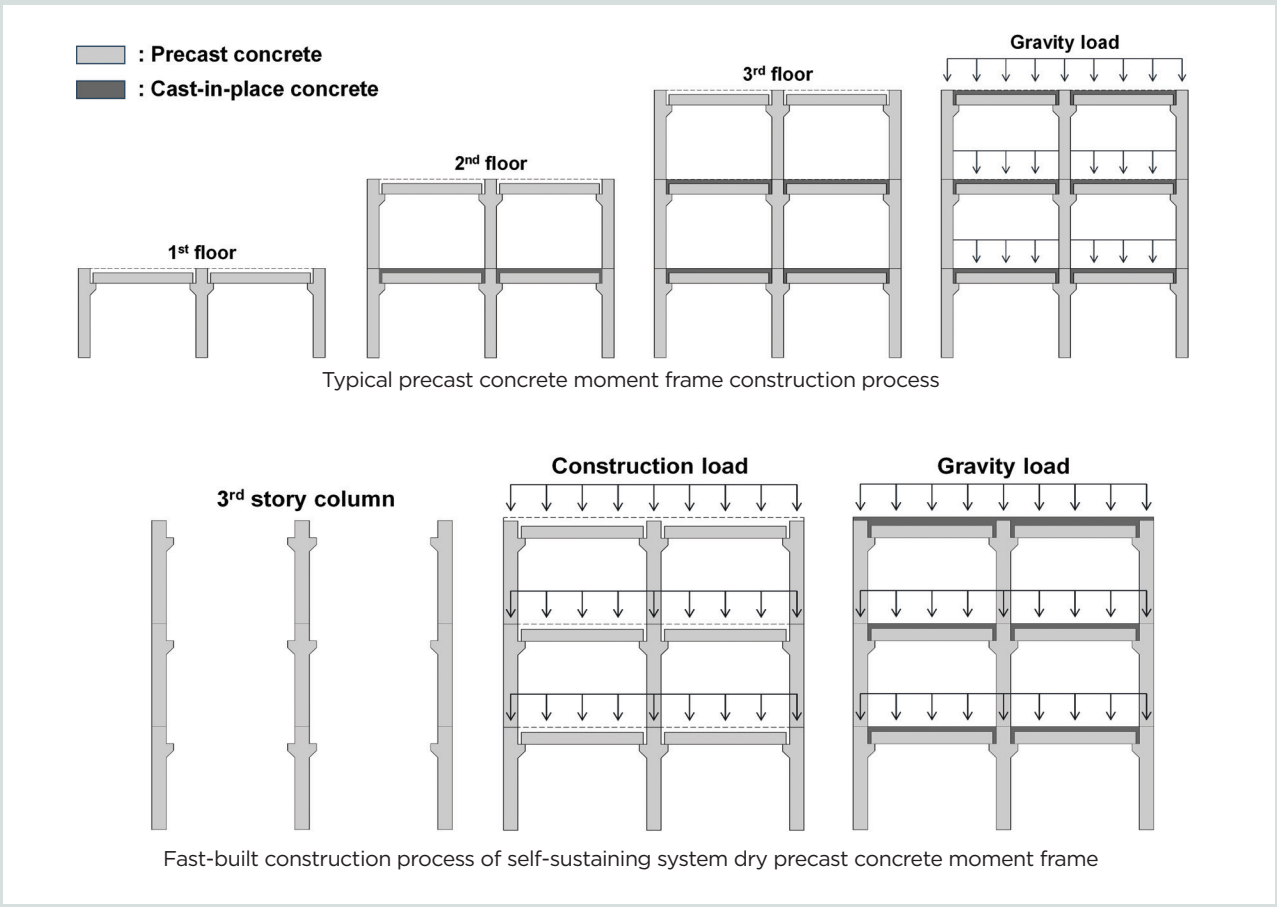

Figure 2. Two modes of construction of a multistory building with a moment frame: Conventional, wet-splicing precast concrete process and self-sustaining dry precast concrete system.

- rotating couplers (within topping concrete)
- single-head couplers (at top reinforcement of precast concrete beams)
- double-head couplers (at bottom reinforcement of precast concrete beams), where the solid panel zone is already built into the bottom precast concrete column component (This means the connecting longitudinal reinforcing bars cannot be rotated and fastened by themselves because they are already fully bonded in the precast concrete beams and the solid panel zone.)

First, the rotating coupler can be used only when the reinforcing bars can be freely rotated to tighten the cap. However, for rapid construction of upper floors, a solid panel zone is required (Fig. 1). To this end, new coupler systems were devised to connect the reinforcing bars that are preinstalled (bonded) in precast concrete components and cannot be freely rotated for screw-tightening. Each dry mechanical splice consists of an external holder and corresponding tightening cap with one or two internal heads (single- or double-head coupler, respectively). As Fig. 3 shows, the external holder is embedded in the precast concrete column (that is, the solid panel zone), and an internal head is threaded onto the reinforcing bars, which is then locked by fastening the tightening cap, thereby achieving fully code-compliant splice performance. In the single-head coupler configuration (Fig. 3), the external holder is embedded in the precast concrete column and the internal head with a threaded auxiliary (short) bar is positioned and then locked with the tightening cap to ensure reinforcement continuity. Similarly, in the double-head coupler configuration, short auxiliary bars with internal heads protrude from both the precast concrete beam and the precast concrete column and bear against each other; the external holder is then fastened to complete the assembly. Fig. 3 also illustrates the dry splice detail for column splices. Although the fastening procedure is similar to that of the rotating coupler, the internal head is extended to improve constructibility under typical on-site erection conditions. For a clearer understanding of the connection mechanism, a demonstration video is available on YouTube.[12]

In summary, the external holder–tightening cap assembly transfers tension and resists compression through head-to-head or head-to-holder bearing action. Because the internal head is manufactured to have a larger diameter than the connecting reinforcing bars, a tolerance of more than 5 mm (0.2 in.) in any radial direction of the connecting bar can be

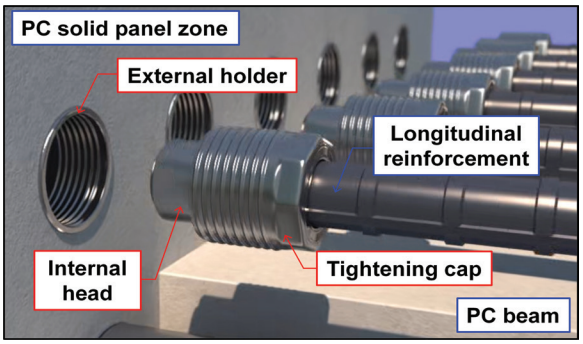

Rotating coupler

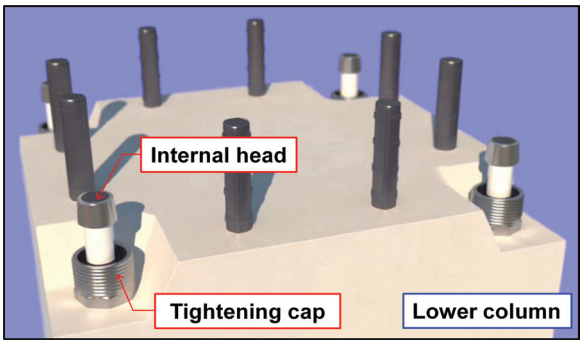

Lower column

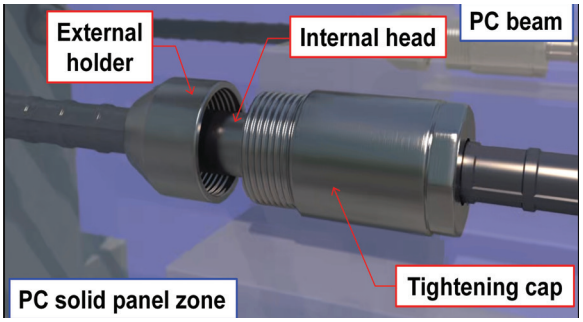

Single-head coupler

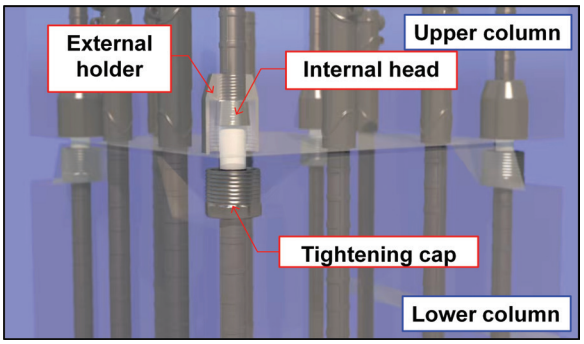

Vertical mechanical coupler

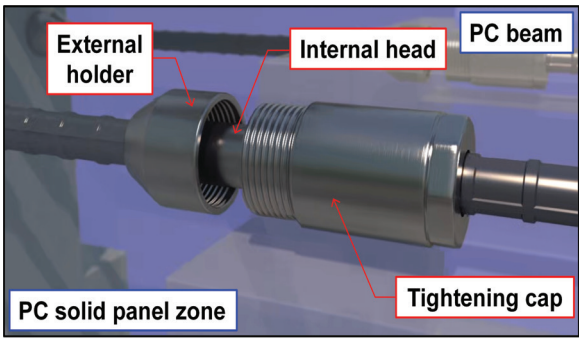

Double-head coupler

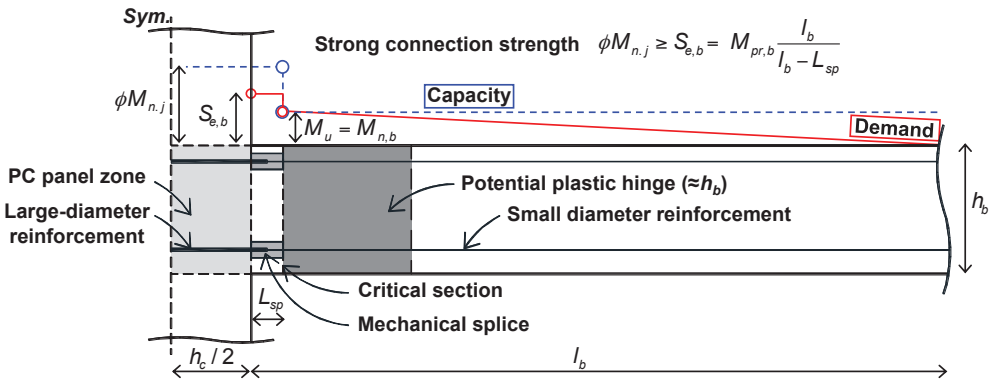

Design concept of strong connection

Figure 3. Details of dry mechanical splices and a design concept of a strong connection. Note: h_b = depth of beam; h_c = depth of column; l_b = single-beam span length; L_{sp} = length of mechanical splice; $M_{n,b}$ = nominal flexural strength of beam section; $M_{pr,b}$ = probable flexural strength of beam; M_u = factored flexural moment of beam; PC = precast concrete; $S_{e,b}$ = probable flexural strength; Sym. = symmetric; $\phi M_{n,j}$ = design flexural strength of strong connection.

easily secured. This tolerance range is comparable to that typically accommodated in grouted-sleeve systems used in precast concrete construction. Therefore, the proposed dry splice does not require unusually tight field-alignment control.

In addition, the inner surface of the holder and back side of internal heads are designed to be in contact to properly fasten the external holder with the tightening cap so that on-site quality control is also easily attained. Although the holder–cap assembly is tightened manually, tightening quality can be ensured through a simple field procedure. Specifically, after confirming firm head-to-head contact, the tightening cap is fastened into the embedded holder until full thread engagement is achieved, which can be verified by a visual check that no external threads remain exposed after tightening. The holder is embedded in the precast concrete column, and during on-site assembly, enough threaded engagement length of the internal head is provided that it can be adjusted to achieve firm contact with the internal head from another side or external holder,[12] after which the holder and tightening cap are secured. The proposed mechanical splice system incorporates an internal head threaded onto the reinforcing bar with an effective bearing area greater than the cross-sectional area of connecting bars to ensure adequate safety under head-to-head contact.

The proposed self-sustaining dry precast concrete system creates a code-compliant strong connection. Section 18.9.2.2 of the American Concrete Institute's *Building Code for Structural Concrete—Code Requirements and Commentary*,[13] ACI CODE-318-25, specifies that two connecting reinforcements with different diameters need to be mechanically spliced in a tight manner. During the assembly of the precast concrete components, construction tolerances can be effectively accommodated, and fastening the external holder and cap achieves reinforcement continuity and reliable stress-transfer performance at the splice. And, as previously explained, because the precast concrete system has a high self-sustaining capacity, temporary supports are not required during erection, allowing for rapid and efficient construction.

Test specimens

The experimental program consisted of two precast concrete specimens designated as the P series and two cast-in-place specimens with monolithic connection details designated as the R series. Each specimen was proportioned and detailed to represent either a portion of a special or intermediate moment frame system—designated S or I, respectively—specified in chapter 18 of ACI CODE-318-25[13] and *Structural Precast Concrete—Code Requirements and Commentary*,[14] ACI/PCI 319-25. All test specimens shared similar overall geometric configurations, except for a corbel required for erection in the precast concrete specimens. The corbel primarily served as a beam-seating/erection feature, and although it may influence local load transfer near the joint, the global cyclic response metrics compared in this study were not materially affected under the tested conditions.

All test specimens were designed in accordance with the strong column–weak beam philosophy except for the different levels of overstrength addressed in precast concrete joints depending on the target seismic force-resisting system (that is, special and intermediate moment frame systems). The applied seismic design provisions included the requirements for beams, columns, joints, reinforcement development, and splices. For the PS specimen, the special beam–column joint details were made to be code compliant based on the strong connection so that the plastic hinge regions of the beam are intentionally formed outside of the mechanical splice region. (Refer to section 18.9.2.2 of ACI CODE-318-25[13] and ACI/PCI 319[14]). In a joint designed to be the strong connection, the longitudinal reinforcement of the beam passing through the panel zone must maintain continuity beyond the plastic hinge region. Accordingly, the design flexural strength of the strong connection $\phi M_{n,j}$ as part of the special precast concrete moment frame system specified in ACI CODE-318-25 and ACI/PCI 319 shall be not less than coexisting design forces including shear when the critical section reaches the probable flexural strength $S_{e,b}$, which can be expressed, as follows:[15]

$$\phi M_{n,j} \geq S_{e,b} = M_{pr,b} \frac{l_b}{l_b - l_{sp}} \quad (1)$$

where

$M_{pr,b}$ = probable flexural strength of the beam at the critical section, calculated using $1.25f_y$

l_b = single-beam span length = 2250 mm

l_{sp} = mechanical coupler length = 160 mm

f_y = specified yield strength of nonprestressed reinforcement

In this study, the beam–column joint detail of the PS specimen was designed in accordance with Eq. (1), which indicates that two connecting reinforcing bars with different diameters must be mechanically spliced—one extending from the panel zone and the other from the precast concrete beam—to ensure adequate overstrength in flexure and shear friction at the precast concrete joint (Fig. 3). This emphasizes the design requirement for mechanical splicing of bars with different diameters.

Figure 4 shows the configuration and reinforcement details of the PS and PI specimens (the precast concrete specimens). The height and length of the test specimens were set to be 3220 and 6000 mm (10.6 and 19.7 ft), respectively. This test subassembly was designed as a half-scale representation of a prototype beam–column joint to satisfy laboratory constraints while preserving the intended detailing and response mechanisms.

All of the columns in the precast concrete specimens were spliced at the top level of topping concrete of the precast

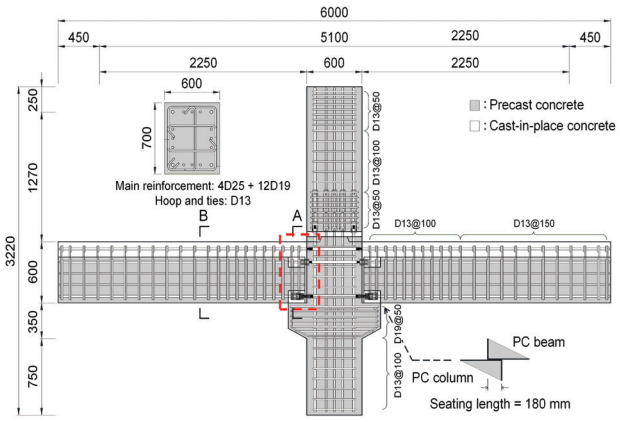

Elevation of precast concrete specimens

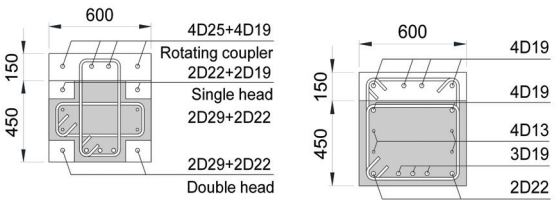

A-A section B-B section

Beam details of PS specimen

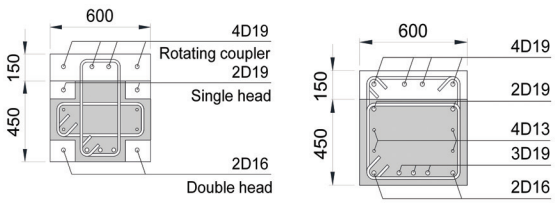

A-A section B-B section

Beam details of PI specimen

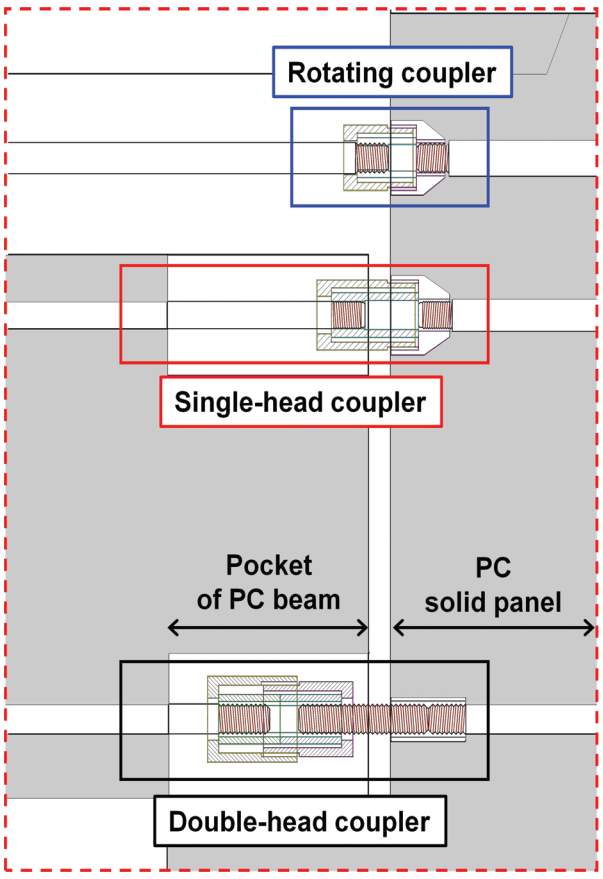

Details of mechanical splicing in precast concrete panel zone

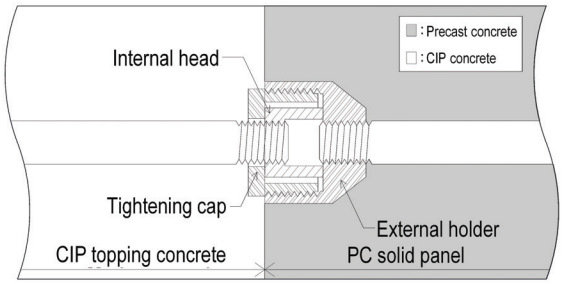

Rotating coupler

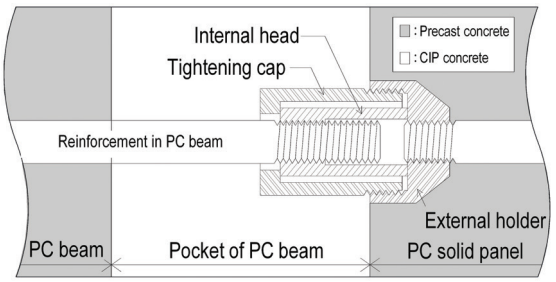

Single-head coupler

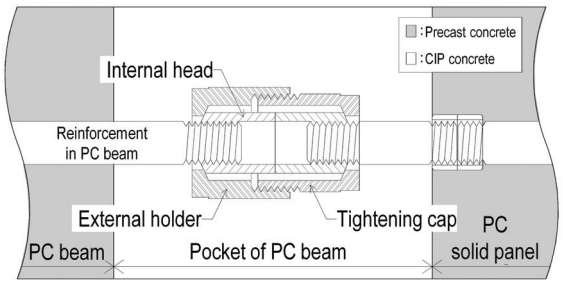

Double-head coupler

Figure 4. Configuration and reinforcement details of precast concrete specimens. Note: All measurements are in millimeters. CIP = cast in place; PC = precast concrete; PI = precast concrete intermediate moment frame system; PS = precast concrete special moment frame system. 1 mm = 0.039 in.; D13 = no. 4 = 13M; D16 = no. 5 = 16M; D19 = no. 6 = 19M; D22 = no. 7 = 22M; D25 = no. 8 = 25M; D29 = no. 9 = 29M.

concrete beams, where four corner reinforcements were connected by the dry mechanical splices and other reinforcements were spliced with conventional grout sleeves. The lower precast concrete column includes a prefabricated solid panel zone for fast and self-sustaining construction (Fig. 1).

In the PS specimen with the special seismic details, the longitudinal bars preinstalled in the solid panel zone of the precast concrete column were substantially larger than the beam longitudinal bars in order to satisfy the strong connection requirement specified in ACI CODE-318-25.[13] Specifically, in the region where the double-head couplers were applied, the bars passing through the panel zone were D29 (no. 9 [29M]), whereas the precast concrete–beam bars were D22 (no. 7 [22M]). ACI CODE-318-25's strong connections requirement was fully satisfied so that the larger bars in the solid panel zone can remain elastic and a plastic mechanism can be developed in the beam reinforcement that has a smaller diameter.

On the other hand, in the PI specimen with intermediate seismic details based on section 18.4 of ACI CODE-318-25[13] and ACI/PCI 319,[14] the bar size passing through the solid column was set to be the same as that used in the precast concrete beams. The heights of the upper and lower columns were 1420 and 1750 mm (55.9 and 68.8 in.), respectively. The lower column integrated the bracket and panel zone as a single precast concrete component, thereby avoiding the need for cast-in-place concrete within the solid panel zone, improving joint integrity, and enabling fast construction. The precast concrete beam had a square cross-section of 600 mm (23.6 in.) and a total length of 2680 mm (105.5 in.). A bearing length of 180 mm (7.0 in.) at each beam end was seated on the lower-column bracket. The precast concrete beam depth prior to topping was 450 mm (17.7 in.), and the overall composite depth after topping was 600 mm (23.6 in.). All the longitudinal reinforcement of the precast concrete beam passing through the panel zone was connected using dry mechanical splices. Two sets of single-head couplers and two sets of double-head couplers were used for the top and bottom reinforcement of the precast concrete beam, respectively, whereas four rotating couplers were adopted for reinforcement located within the cast-in-place topping concrete region.

Figure 5 presents the configuration and reinforcement details of the RS and RI specimens. These cast-in-place specimens were designed to match the precast concrete specimens in overall dimensions and flexural capacity. The longitudinal reinforcement of the cast-in-place columns and beams was arranged continuously in accordance with conventional cast-in-place construction practice, and the components were designed to provide flexural and shear capacities comparable to those of the precast concrete specimens.

Figure 6 summarizes the fabrication sequences for the precast concrete specimens, which reflect the practical process used in dry precast concrete construction. The precast concrete beams and columns were fabricated separately. At the column-to-column splice at the top level of the precast concrete composite beam sections, dry vertical couplers located at the four corners of the precast concrete column enabled self-supporting capacity without the need for temporary shoring. The precast concrete beam was then seated on its bracket, and horizontal mechanical splices were tightened to maintain continuity of the beam reinforcement through the panel zone and

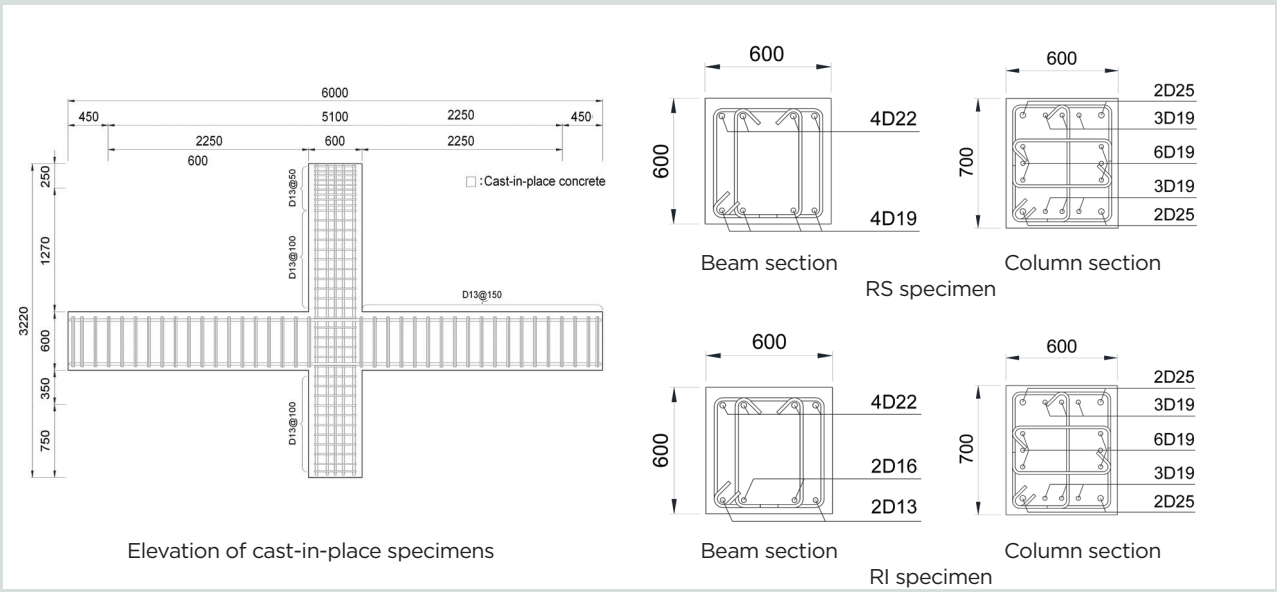

Figure 5. Configuration and reinforcement details of cast-in-place concrete specimens. Note: All measurements are in millimeters. RI = cast-in-place concrete intermediate moment frame system with monolithic connection details; RS = cast-in-place concrete special moment frame system with monolithic connection details. 1 mm = 0.039 in.; D13 = no. 4 = 13M; D16 = no. 5 = 16M; D19 = no. 6 = 19M; D22 = no. 7 = 22M; D25 = no. 8 = 25M.

Precast concrete component

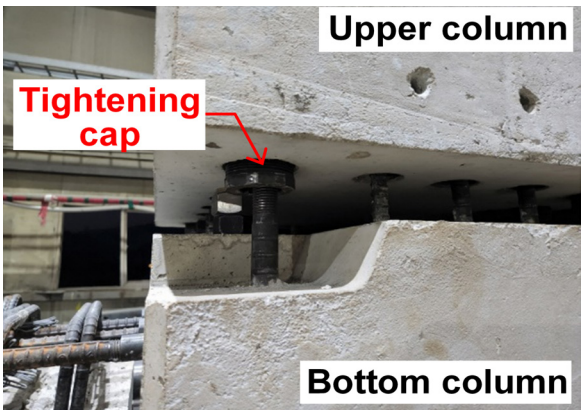

Vertical coupler

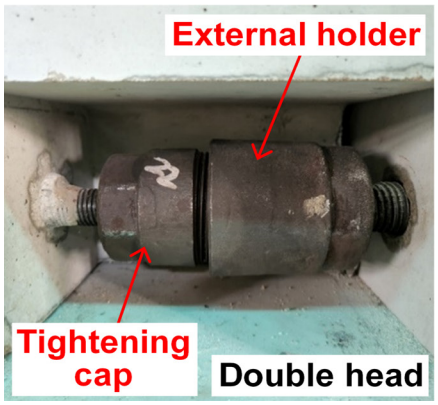

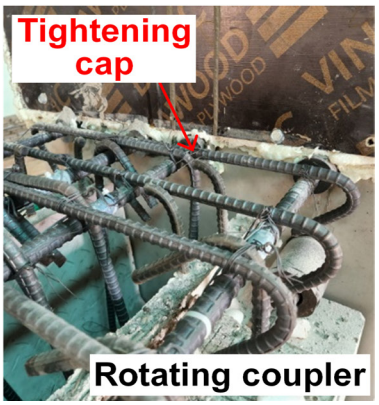

Horizontal coupler

Cast-in-place concrete

Precast concrete beam-column connections

Figure 6. Manufacturing process of precast concrete beam–column connections specimens. Note: PC = precast concrete.

beyond the plastic hinge region. After assembly, high-strength and high-flow grout was injected into the splice sleeves in the column except for the dry couplers at the four corners, and cast-in-place concrete was placed onto the roughened top surface of the precast concrete beams to ensure composite action. For the cast-in-place specimen series, all connections were cast monolithically with no splice between reinforcements.

Material properties

Material tests on concrete cylinders and reinforcing bars were conducted on the day of the structural tests. **Table 1** summarizes the average compressive strengths of the concrete and grout. The concrete compressive strength for the precast concrete columns and beams was identical and measured at 37.3 MPa (5410 psi), whereas the cast-in-place concrete

Table 1. Average compressive strength of concrete and grout

Specimen	Concrete compressive strength f'_c, MPa			Grout compressive strength f'_g, MPa
	Precast concrete beam	Cast-in-place beam	Column	
PS	37.3	36.8	37.3	61.4
PI	37.3	33.3	37.3	61.4
RS	n/a	35.9	35.9	n/a
RI	n/a	34.7	34.7	n/a

Note: n/a = not applicable; PI = precast concrete intermediate moment frame system; PS = precast concrete special moment frame system; RI = cast-in-place concrete intermediate moment frame system with monolithic connection details; RS = cast-in-place concrete special moment frame system with monolithic connection details. 1 MPa = 0.145 ksi.

ranged from 33.3 to 36.8 MPa (4830 to 5340 psi). The cube strength of the grout was 61.4 MPa (8900 psi).

Extensive tensile tests were conducted for both the bare bars and the mechanically spliced bar systems with various combinations of the mechanical splice systems used in the precast concrete specimens (for example, vertical coupler, double-head coupler, single-head coupler, and rotating coupler). **Figure 7** and **Table 2** present the results of these tests. The specified yield strength of D25 (no. 8 [25M]) reinforcement was 500 MPa (72.5 ksi), whereas that of the other bars used in the test specimens was 400 MPa (58.0 ksi). For all the specimens, yielding and fracture occurred in the reinforcing bar outside of the mechanical splice device, and no significant differences were observed among the test results. The proposed mechanical splice details fully satisfied the performance requirements for the Type 2 mechanical splice specified in ACI CODE-318-25.[13] No cyclic test was conducted to check Grade S performance because this new provision (in ACI CODE-318-25) was not available at that time. Instead, as Fig. 7 shows, the proposed mechanical splices fully satisfy the Korean performance criteria of the high-stress cyclic loading test, as specified in KS D 0249, *Method of Inspection for Mechanical Splicing Joint of Bars for Concrete Reinforcement*[16] (the test method for mechanical splices of reinforcing steel bars for reinforced concrete), where the slip between reinforcement and splice device was less than 0.3 mm (0.1 in.) and passed the seismic application criterion.

Test setup and loading protocol

Figure 8 presents the test setup and loading protocol. The column base was set to be a pin support, and roller supports were provided at both ends of the beam. The distance between the roller supports (the beam span length L_b) was 5.10 m (16.7 ft). The lateral load was applied at a point 250 mm (9.8 in.) below the top of the column by a displacement-controlled actuator with a 2000 kN (449.6 kip) capacity. This loading protocol follows *Acceptance Criteria for Moment Frames Based on Structural Testing and Commentary*, ACI 374.1-05.[17] To simulate the gravity load in an actual structure, an axial load equal to 10% of the design axial strength of the column (1470 kN [330.5 kip]) was applied at the top of the column prior to applying lateral cyclic loads. Considering the effective column height h_{eff} of 3170 mm (124.8 in.), 12 drift stages from 0.2% to 6.0% were imposed with three repeated cycles at each level in both the positive (push, plus sign) and negative (pull, minus sign) directions. For the test specimens that did not exhibit a strength drop below 80% of the peak load (before the ultimate point), a single additional loading step to a

Table 2. Properties of reinforcement and mechanical splice: Results of tensile testing

	Reinforcing bar						Mechanical splice				
	D13, MPa	D16, MPa	D19, MPa	D22, MPa	D25, MPa	D29, MPa	Vertical coupler, MPa		Single head, MPa	Double head, MPa	Rotating coupler, MPa
							D25	D22			
f_y	400	400	400	500	500	400	500	500	400	400	400
$f_{y.test}$	517.1	504.9	511.2	508.5	522.1	469.8	610.4	594.1	507.1	540.8	519.5
$f_{u.test}$	670.4	729.7	658.7	641.0	717.9	636.8	692.8	705.0	664.1	661.8	665.4
Yield ratio $f_{y.test}/f_{u.test}$	1.29	1.44	1.28	1.26	1.37	1.35	1.13	1.18	1.30	1.22	1.28

Note: $f_{u.test}$ = tensile strength of the reinforcement; f_y = specified yield strength of nonprestressed reinforcement; $f_{y.test}$ = yield strength of the reinforcement. 1 MPa = 0.145 ksi; D13 = no. 4 = 13M; D16 = no. 5 = 16M; D19 = no. 6 = 19M; D22 = no. 7 = 22M; D25 = no. 8 = 25M; D29 = no. 9 = 29M.

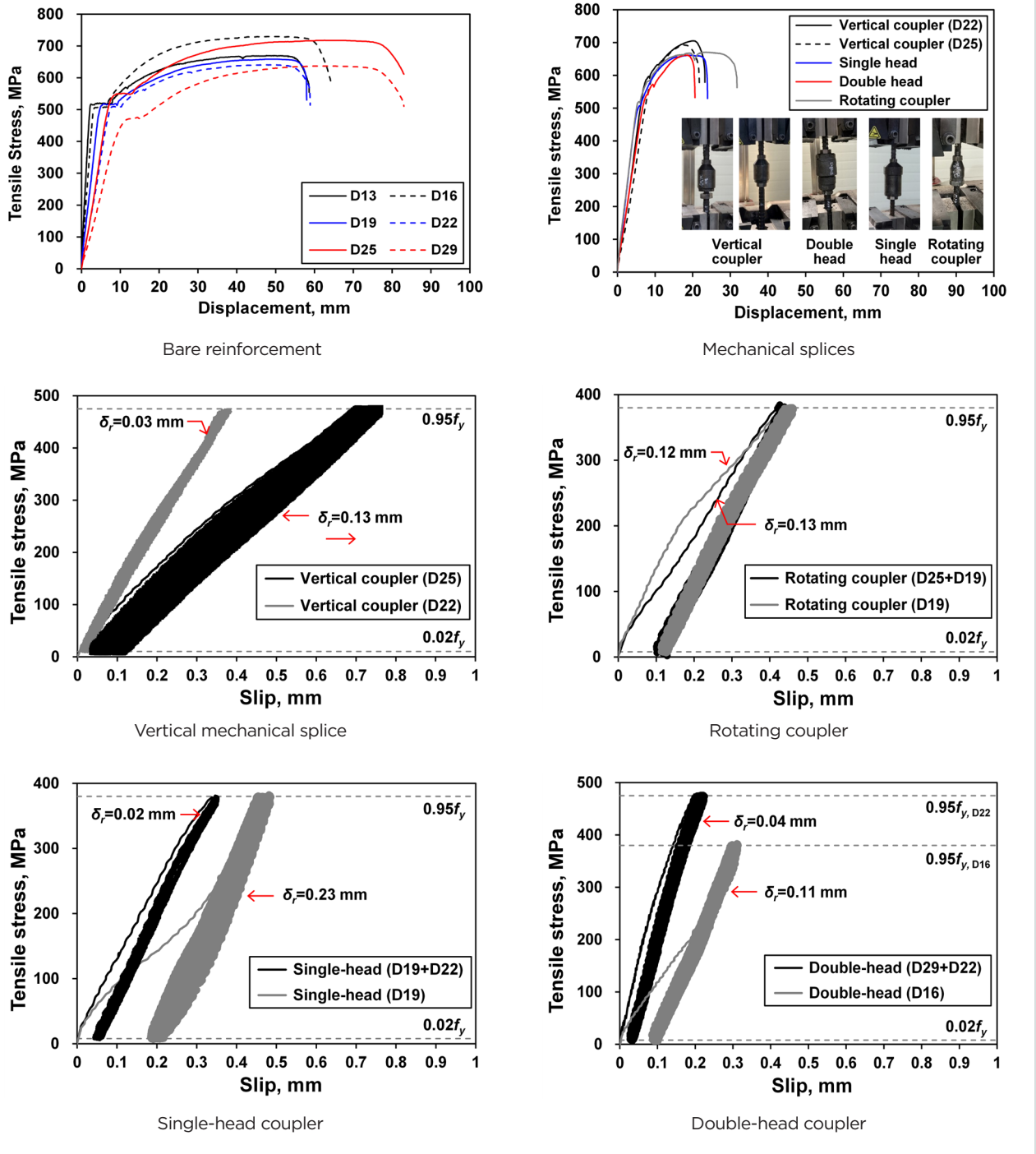

Figure 7. Results of tensile testing of reinforcing bars and mechanical splices. Note: f_y = specified yield strength of nonprestressed reinforcement; δ_r = residual displacement of the mechanical splice. 1 mm = 0.039 in.; 1 MPa = 0.145 ksi; D13 = no. 4 = 13M; D16 = no. 5 = 16M; D19 = no. 6 = 19M; D22 = no. 7 = 22M; D25 = no. 8 = 25M; D29 = no. 9 = 29M.

7.0% drift ratio was applied. Linear variable displacement transducer (LVDT) 1 was installed to monitor the global horizontal displacement of the specimen and LVDTs 2 to 4 were also installed to track any slip at the supports so that the target displacement at each drift level could be corrected in real time.

Experimental results

Strength and cyclic response

All test specimens were designed according to the strong column–weak beam philosophy. **Table 3** presents the calcu-

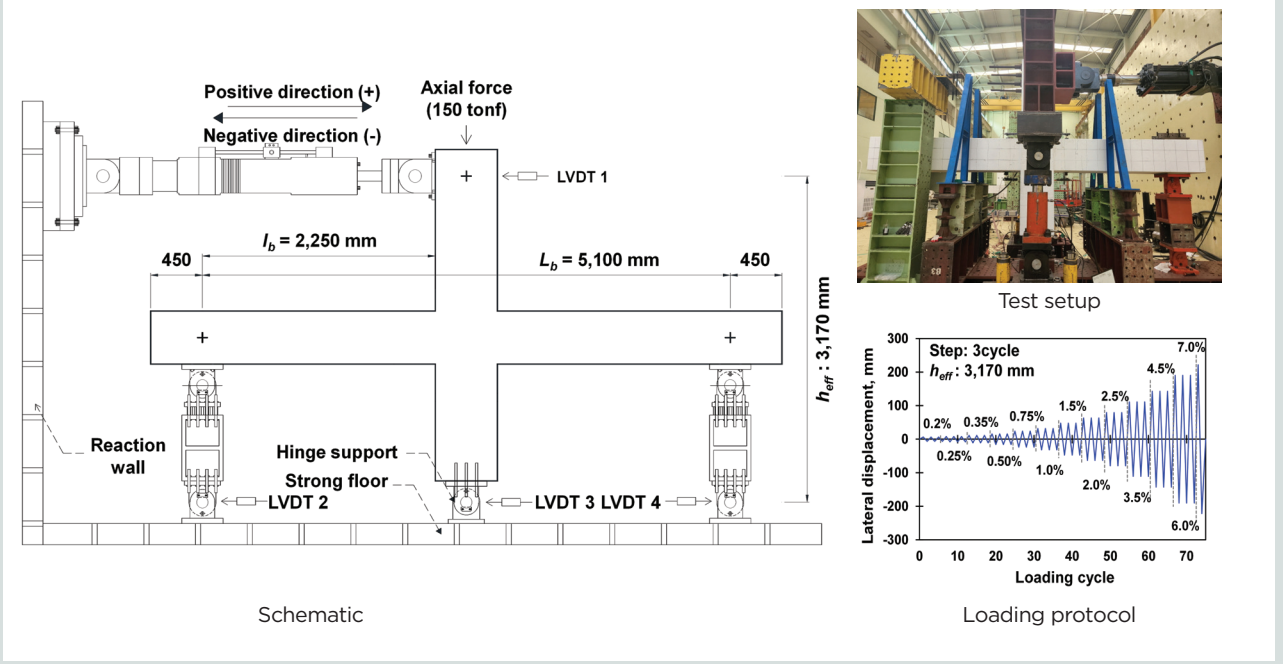

Figure 8. Test setup and loading protocol. Note: All measurements are in millimeters. h_{eff} = effective column height; l_b = single beam span length; L_b = beam span length; LVDT = linear variable displacement transducer. 1 mm = 0.039 in.; 1 tonf = 9.8 kN = 2.2 kip.

Table 3. Comparisons of test and capacity calculation results

Variable tested	Special moment frame		Intermediate moment frame	
	PS	RS	PI	RI
$M_{n,b}$, kN-m	268.0 (-414.4)	292.6 (-402.8)	166.6 (-428.7)	177.7 (-415.3)
$M_{n,c}$, kN-m	633.2	618.2	465.7	450.1
$\Sigma M_{n,c}/\Sigma M_{n,b}$	1.86	1.78	1.56	1.52
Q_n, kN	246.2 (-246.2)	248.6 (-248.6)	214.7 (-214.7)	212.0 (-212.0)
V_{jh}, kN	1350.6	1469.2	1121.3	1146.9
V_{jn}, kN	3649.8	3580.6	3649.8	3520.3
V_{jh}/V_{jn}	0.370	0.410	0.307	0.326
$S_{e,b}$, kN-m	360.6 (-557.7)	n/a	n/a	n/a
$\phi M_{n,j}$, kN-m	381.8 (-606.1)	n/a	n/a	n/a
$\phi M_{n,j}/S_{e,b}$	1.06 (1.08)	n/a	n/a	n/a

Note: Numbers in parenthesis denote negative direction values. $M_{n,b}$ = nominal flexural strength of beam section; $M_{n,c}$ = nominal flexural strength of column section; n/a = not applicable; PI = precast concrete intermediate moment frame system; PS = precast concrete special moment frame system; Q_n = nominal lateral-load capacity of specimen; RI = cast-in-place concrete intermediate moment frame system with monolithic connection details; RS = cast-in-place concrete special moment frame system with monolithic connection details; $S_{e,b}$ = probable flexural strength; V_{jh} = maximum joint shear force; V_{jn} = joint shear strength; $\phi M_{n,j}$ = design flexural strength of strong connection. 1 kN = 0.225 kip; 1 kN-m = 0.738 kip-ft.

lated nominal flexural strengths of the beam $M_{n,b}$ and columns $M_{n,c}$. All specimens exhibited a column-to-beam nominal flexural strength ratio of at least 1.2, indicating that the intended strong column–weak beam design philosophy was satisfied.

Using the nominal beam flexural strength $M_{n,b}$ with the target yielding location in the beam (that is, the critical section), the nominal lateral-load capacity of the test specimens Q_n can be estimated as follows:

$$Q_{n.PC} = \left(M_{n,b}^{+} + M_{n,b}^{-}\right)\frac{L_b}{h_{eff}} / \left(L_b - h_{co} + 2s\right)$$

where

$M_{n,b}^{+}$ = positive nominal flexural strength of the beams

$M_{n,b}^{-}$ = negative nominal flexural strength of the beams

h_{co} = bracket depth

s = seating length of the precast concrete beam

$$Q_{n.RC} = \left(M_{n,b}^{+} + M_{n,b}^{-}\right)\frac{L_b}{h_{eff}} / \left(L_b - h_c\right)$$

where

h_c = depth of column

For the cast-in-place beam–column connection, the nominal strength was calculated excluding the beam seating length.

For the joint shear strength in the joint panel zone, the maximum joint shear force V_{jh} is determined based on force equilibrium as follows:

$$V_{jh} = T_1 + T_2 - Q_n = \alpha(A_{s1}f_y + A_{s2}f_y) - Q_n$$

where

T_1 = maximum tensile force in the tension reinforcement of left beam

T_2 = maximum tensile force in the tension reinforcement of right beam

α = stress multiplier that accounts for the increased flexural strength due to strain hardening, typically taken as 1.25

A_{s1} = total cross-sectional areas of the tension reinforcement in left beam

A_{s2} = total cross-sectional areas of the tension reinforcement in right beam

In accordance with the seismic provisions of *Recommendations for Design of Beam-Column Connections in Monolithic Reinforced Concrete Structures*, ACI 352R-02,[18] the joint shear strength V_{jn} at the panel zone can be taken as follows:

$$V_{jn} = 0.083\gamma\sqrt{f'_c}b_j h_c$$

where

γ = coefficient addressing the confinement effect of the beams framed into the joint based on the specimen geometry = 20

b_j = effective width of the joint transverse to the direction of shear

As Table 3 shows, V_{jn} for all specimens significantly exceeded V_{jh}; therefore, the potential of joint panel zone shear failure after beam yielding was evaluated to be negligible. As noted previously, the strong connection for the precast concrete special moment frame should be checked using Eq. (1). Using the material test results, the required values were calculated and the PS specimen was found to satisfy the strong connection criterion.

Figure 9 shows the lateral load–story drift ratio relationships of the precast and cast-in-place concrete specimens. An idealized elastic–perfectly plastic response was defined by connecting the yield point and the ultimate point.[19–21] The yield and ultimate points were defined using the same bilinear idealization procedure for all specimens, with positive and negative directions evaluated consistently. The solid blue line represents the backbone curve obtained by connecting the peak-load points at each loading step, whereas the red dashed line represents the idealized elastic–perfectly plastic response defined by the line connecting the yield point and ultimate point. **Table 4** summarizes the key test results, and **Figure 10** presents the ultimate crack patterns and failure modes.

In the precast concrete specimen series, flexural cracks initiated in the precast concrete beams at early loading stages, and joint shear cracks were observed right after beam yielding. Unlike the PI specimen, the PS specimen designed under the strong connection concept exhibited numerous beam flexural cracks forming outside the mechanical splice region. No distinct damage or bar slip was observed at the mechanical splices, ensuring the integrity and continuity of the longitudinal beam reinforcements through the solid panel zone. For the PS and PI specimens, the failure mode was flexure dominated, occurring during loading at story drift ratios of 4.5% for the PS specimen and 7.0% for the PI specimen, because of the tensile fracture of the beam longitudinal reinforcement and concrete crushing. As intended, the failure mode was governed by tensile fracture of the reinforcement located outside of the mechanical splice region (Fig. 10). The cast-in-place series specimens exhibited typical hysteretic behavior of monolithic connections with no significant strength degradation up to a 3.5% story drift ratio, and the failure mode was governed by beam flexural failure.

Compared with the cast-in-place series, the precast concrete series showed high deformation capacity and substantial overstrength (test peak load of specimen Q_{max} to Q_n). High local stiffness provided by the mechanical splices at the precast concrete beam–column interface contributed to the strength enhancement, indicating satisfactory seismic performance. In particular, the PS specimens showed less pinching after yielding than the RS specimens, which is attributed to the strong connection details and double-head couplers; the external holder–tightening cap connection and internal heads effectively transferred both the tension and compression, thereby reducing

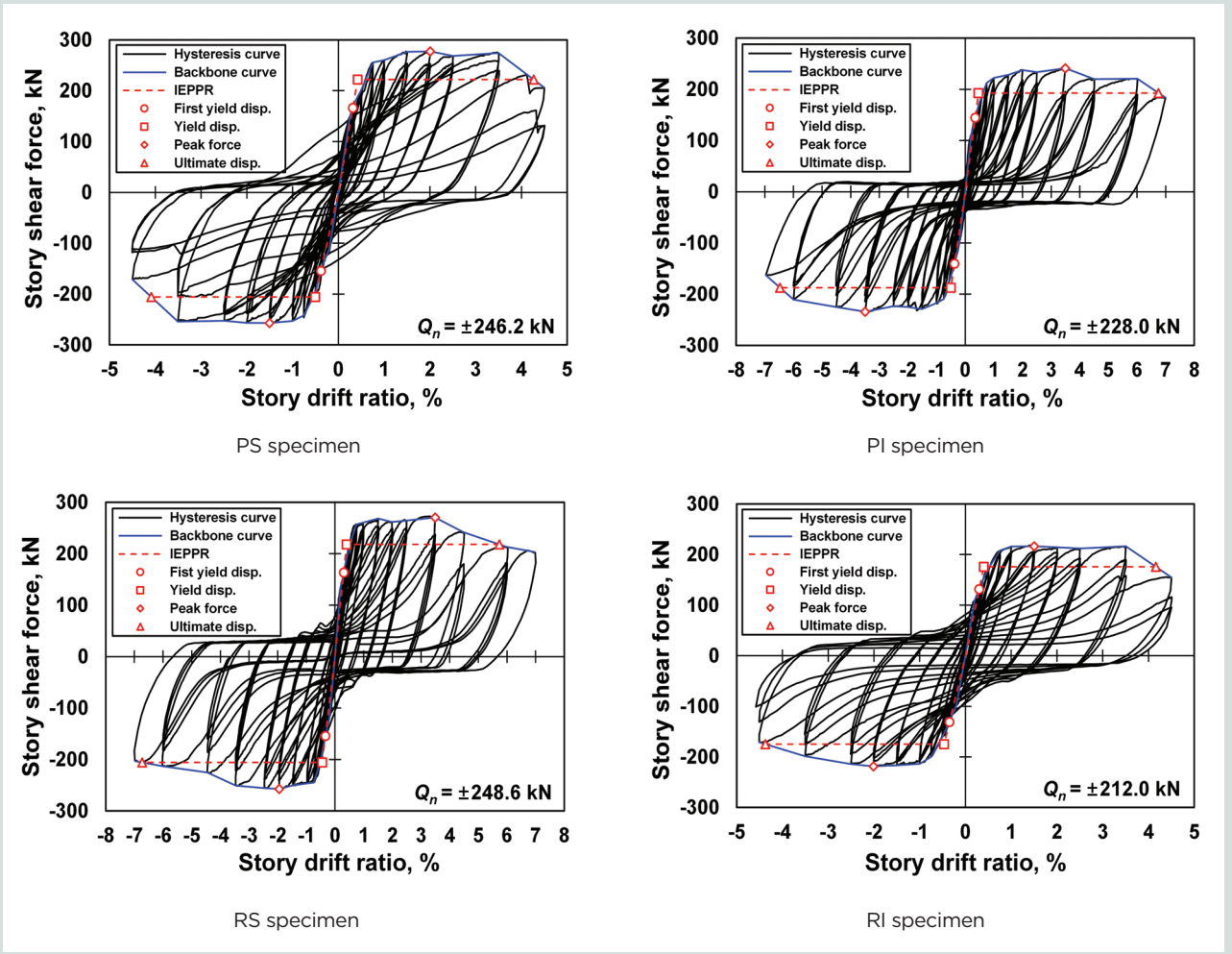

Figure 9. Hysteresis curves of the test specimens. Note: disp. = displacement; IEPPR = idealized elastic–perfectly plastic response; PI = precast concrete intermediate moment frame system; PS = precast concrete special moment frame system; Q_n = nominal lateral-load capacity of specimen; RI = cast-in-place concrete intermediate moment frame system with monolithic connection details; RS = cast-in-place concrete special moment frame system with monolithic connection details. 1 kN = 0.225 kip.

Table 4. Summary of key test results

Specimen	Special moment frame		Intermediate moment frame	
	PS	RS	PI	RI
Yield load Q_y, kN	221.9 (-205.7)	218.0 (-205.6)	192.8 (-187.3)	175.6 (-174.8)
Story drift ratio at yield load θ_y, %	0.42 (-0.51)	0.40 (-0.44)	0.46 (-0.50)	0.39 (-0.46)
Peak load Q_{max}, kN	277.4 (-257.2)	272.6 (-257.0)	241.0 (-234.2)	219.6 (-218.6)
Q_{max}/Q_n	1.13 (1.04)	1.10 (1.03)	1.12 (1.09)	1.04 (1.03)
Story drift ratio at peak load θ_{max}, %	2.00 (-1.50)	3.50 (–1.95)	3.49 (-3.49)	1.50 (-2.00)
Drift ratio at ultimate displacement θ_u, %	4.26 (-4.09)	5.72 (-6.72)	6.75 (-6.46)	4.16 (-4.37)
Failure mode	Beam flexural	Beam flexural	Beam flexural	Beam flexural

Note: Numbers in parenthesis denote negative direction values. PI = precast concrete intermediate moment frame system; PS = precast concrete special moment frame system; Q_n = nominal lateral-load capacity of specimen; RI = cast-in-place concrete intermediate moment frame system with monolithic connection details; RS = cast-in-place concrete special moment frame system with monolithic connection details. 1 kN = 0.225 kip.

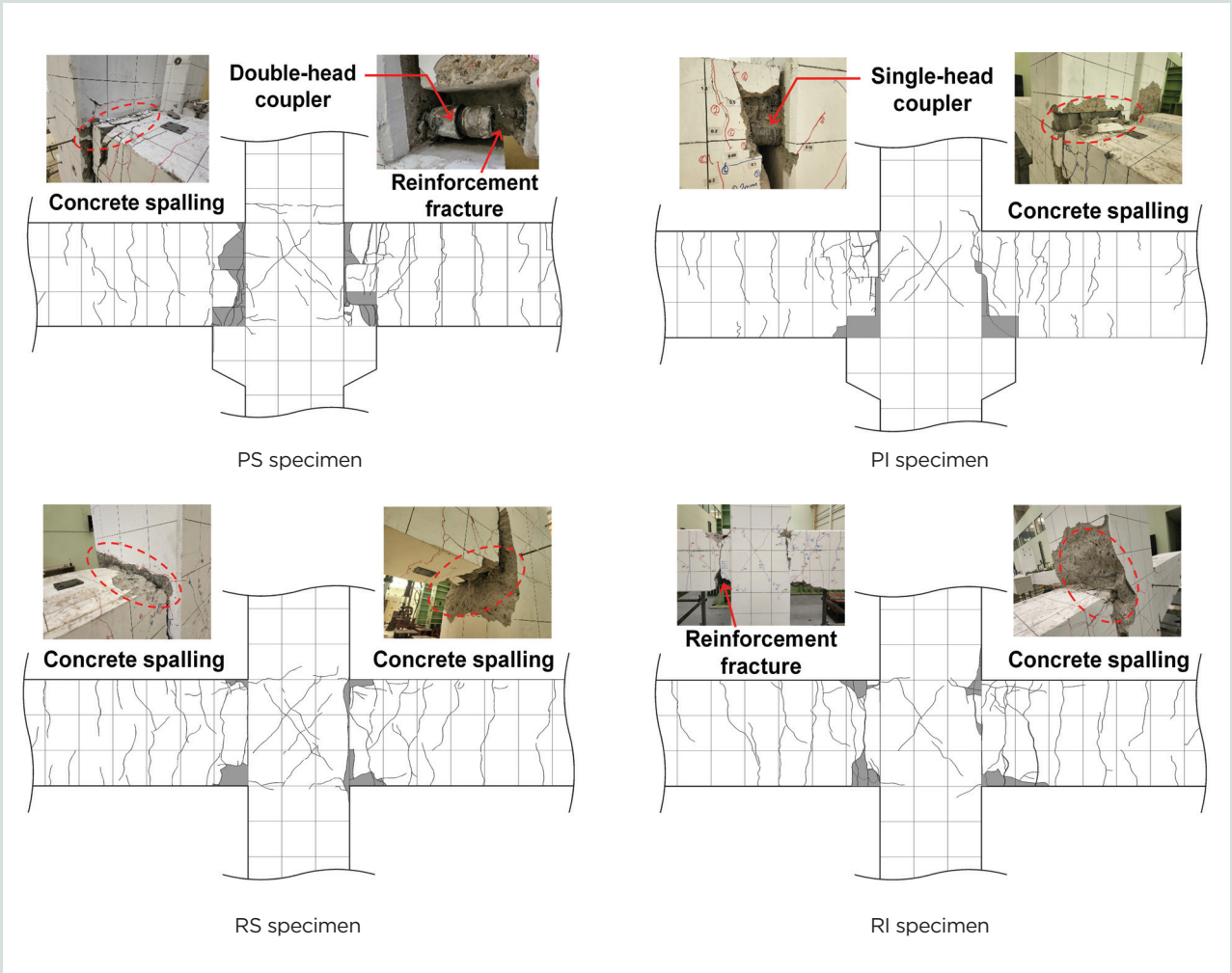

Figure 10. Ultimate crack patterns and failure modes of test specimens. Note: PI = precast concrete intermediate moment frame system; PS = precast concrete special moment frame system; RI = cast-in-place concrete intermediate moment frame system with monolithic connection details; RS = cast-in-place concrete special moment frame system with monolithic connection details.

bond slip. According to ACI 374.1,[17] a beam–column connection specimen for the special moment frame system should retain at least 75% of its peak strength in the third cycle at 3.5% story drift ratio. All the precast concrete specimens fully satisfied this criterion. Accordingly, the precast concrete specimen series showed high load-carrying capacity with no evidence of deficient performance in the mechanical splices.

Strain responses of reinforcement

Figure 11 presents the strain response of the longitudinal reinforcement, in two parts, to identify bar strain responses and the location of the plastic hinge region developed in the beam–column connection.[22–23] The yield strain of the reinforcement was calculated from the actual yield strength obtained in the material tests (Fig. 7). As Fig. 11 shows, strain responses were recorded at the column centerline and at locations 200 and 550 mm (7.8 and 21.6 in.) away from the centerline. At the column centerline (lines A and D), both the precast and cast-in-place concrete specimens exhibited low strains. Strains at lines B and E were higher than those at the centerline. Yielding of the longitudinal reinforcement occurred in the cast-in-place specimens (RS and RI) and in the PI specimen. In contrast, the PS specimen with the strong connection details in accordance with ACI CODE-318-25[13] did not exhibit yielding within the panel zone. Outside the mechanical splice region in the precast concrete specimen series (lines C and F), reinforcement strains showed full yielding for all of the specimens.

To further identify the plastic mechanisms developed along the precast concrete beams of the test specimens, Fig. 11 presents strain profiles of the beam longitudinal reinforcement with respect to selected story drift ratios. At small drift ratios, the bars adjacent to the beam–column interface yielded first. At higher drift demand, the PI, RI, and RS specimens showed yielding of the bars extending through the joint panel zone, but the PS specimens did not show this behavior. The PS specimens provided enough overstrength as required by guidance in ACI CODE-318-25[13] for the capacity design concept.

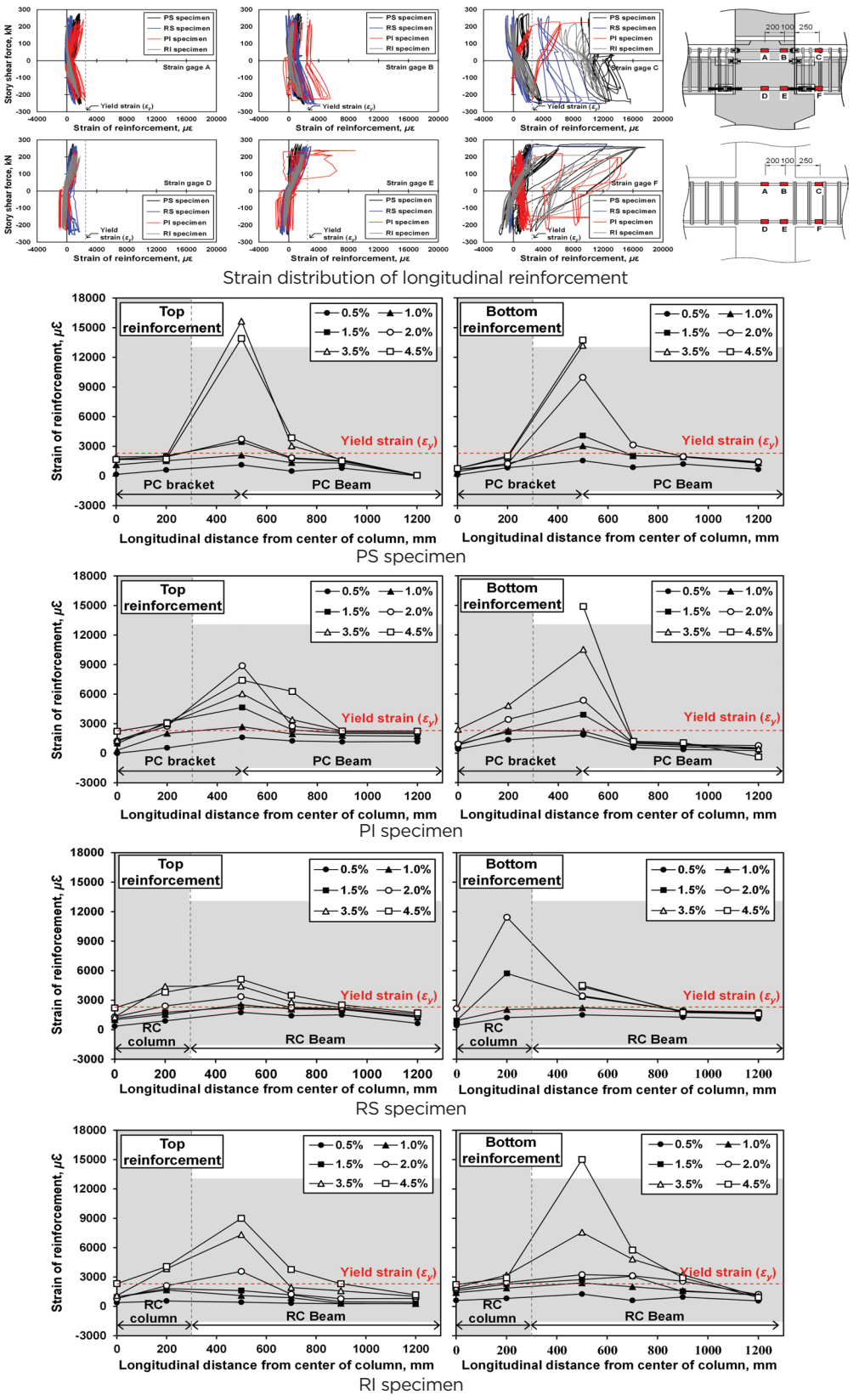

Figure 11. Strain responses of longitudinal reinforcement and plastic hinge regions of beams. Note: PC = precast concrete; PI = precast concrete intermediate moment frame system; PS = precast concrete special moment frame system; RC = reinforced concrete; RI = cast-in-place concrete intermediate moment frame system with monolithic connection details; RS = cast-in-place concrete special moment frame system with monolithic connection details; ε_y = yield strain. 1 mm = 0.039 in.; 1 kN = 0.225 kip.

The test results also indicate that reinforcement strains finally penetrated into the joint region at higher drift levels. In addition, the plastic hinge length of the beam in all specimens was approximately equal to the beam depth h_b. Meanwhile, for the PS specimen, yielding was intentionally developed outside of the mechanical splice region, demonstrating that the plastic hinge mechanism can be relocated as intended using strong connection details for special moment frames in accordance with ACI CODE-318-25.[13]

Energy dissipation capacity

For desirable seismic performance, beams should yield before columns so that sufficient plastic deformation develops in the beams to induce energy-dissipating behavior. This behavior is key to emulative seismic performance of precast concrete structural systems.[24–26] To quantify the energy dissipation capacity of the beam–column specimens, the equivalent viscous damping ratio ξ_{eq} was evaluated at each loading step based on the first enclosed hysteresis loop. The equivalent viscous damping ratio represents the energy dissipated through structural response and can be computed as follows:

$$\xi_{eq} = \frac{1}{4\pi}\frac{E_I}{E_{so}}$$

where

E_I = dissipated energy of a target hysteresis loop

E_{so} = static strain energy for linear-elastic response

Figure 12 shows that the cumulative energy dissipation of the PS, RS, and RI specimens was similar during the early loading stages, whereas the PI specimen exhibited lower energy dissipation after the third cycle, at a 1.0% drift (that is, after more than 18 cycles). This reduction is attributed to earlier attainment of yielding relative to the other specimens, which limited subsequent strength gain and also reduced energy dissipation (Table 4). Regarding the equivalent viscous damping ratios, the precast concrete specimens showed higher damping ratios than the cast-in-place specimens in the plastic region (the ductility capacity of test specimen $\mu > 1$) beyond the elastic range. Based on these findings, the proposed dry mechanical precast concrete connection system exhibits emulative energy-dissipation performance comparable to that of a monolithic system with similar details and dimensions.

Strength degradation

Strength degradation indicates accumulated damage induced by repeated cyclic loading and the corresponding ability of the beam–column joint to maintain load-bearing capacity at a target drift level. As **Fig. 13** illustrates, the strength degradation for each specimen was evaluated by addressing the strength-degradation ratio α_i, where the subscript i denotes the ith loading cycle (for example, the first, second, and third cycle at the same drift level). The strength-degradation ratio α_i at a given story drift ratio is taken as the average value of the positive and negative directions at the peak load of ith cycle.

$$\alpha_i^j = \frac{Q_{i,max}^j}{Q_{1,max}^j}$$

where

j = drift level

i = cycle number at a given drift level

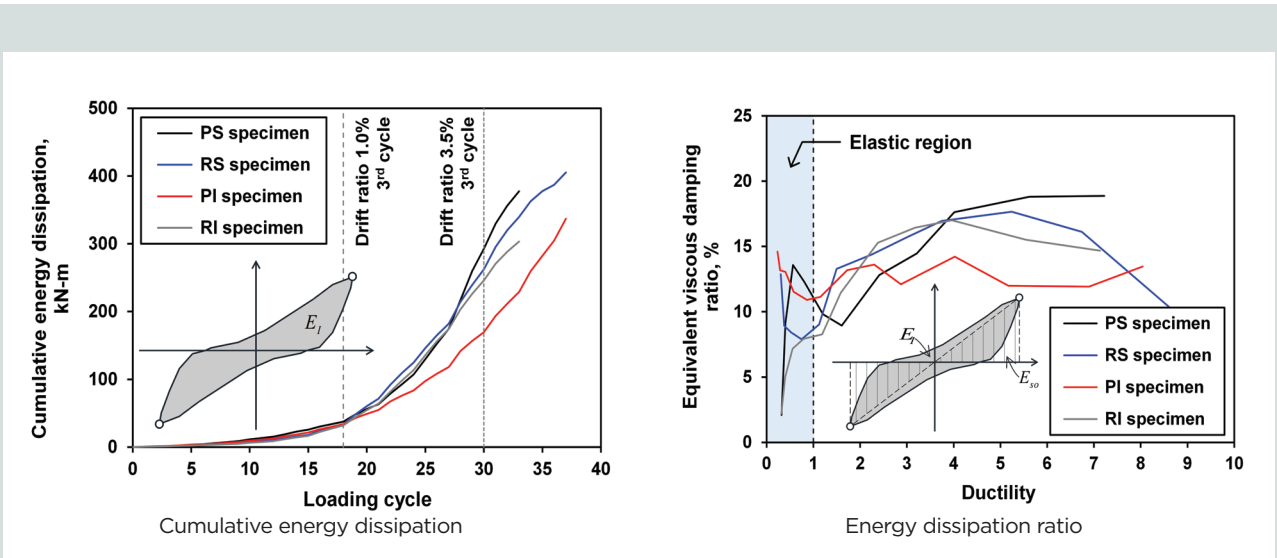

Figure 12. Energy dissipation capacity of the test specimens. Note: E_I = dissipated energy of a target hysteresis loop; E_{so} = static strain energy for linear-elastic response; PI = precast concrete intermediate moment frame system; PS = precast concrete special moment frame system; RI = cast-in-place concrete intermediate moment frame system with monolithic connection details; RS = cast-in-place concrete special moment frame system with monolithic connection details. 1 kN-m = 0.7376 kip-ft.

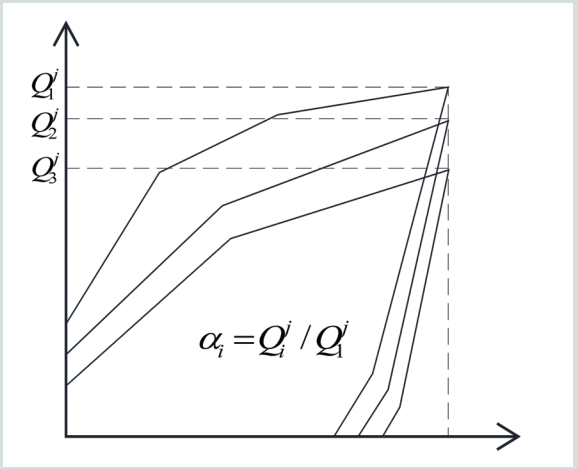

Figure 13. Definition of the strength degradation ratio. Q_i^j = average load of the positive and negative directions in the *i*th cycle at the *j*th drift level; α_i = strength degradation for each specimen was evaluated by addressing the strength-degradation ratio in *i*th loading cycle.

$Q_{i,max}^j$ = average peak load of positive and negative directions in the *i*th cycle at the *j*th drift level

$Q_{1,max}^j$ = average peak load of positive and negative directions in the first cycle at the *j*th drift level

In general, when cracks are well distributed throughout a structural component, strength degradation at the same drift tends to be small. Conversely, when cracking is localized, stiffness drops significantly, and the strength-degradation ratio increases markedly.[27–29] According to ACI 374.1,[17] a beam–column connection specimen must maintain at least 75% of Q_{max} in the third cycle of a 3.5% story drift ratio. **Figure 14** plots the strength-to-degradation ratios for the second cycle α_2 and third cycle α_3 versus each drift ratio, along with linear regression lines. For all specimens, α_i decreased approximately linearly as the drift ratio increased. The ratio for the third cycle α_3 is lower than that of the second α_2, indicating the cumulative strength degradation under repeated load cycling. The RI specimen exhibited a notably steeper regression slope, indicating the higher degradation at large drifts. At the 3.5% drift ratio, the strength-degradation ratio at the third cycle α_3 is 0.80 for the PS specimen and 0.89 for the PI specimen; both specimens satisfied the acceptance criterion. Overall, the precast concrete specimens did not show lower strength-degradation ratios than the cast-in-place specimens.

In **Table 5**, the test results were evaluated in detail using the acceptance criteria of ACI 374.1[17] for moment frame systems based on structural testing. As a result, the overall seismic performance of all specimens satisfied these criteria or was comparable to that of the cast-in-place specimens.

Nonlinear modeling approach

Seismic performance of the precast and cast-in-place concrete beam–column connection specimens can be evaluated using the macromodeling approach in accordance with the nonlinear analysis procedures presented in the American Society of Civil Engineers/Structural Engineering Institute's *Seismic Evaluation and Retrofit of Existing Buildings*, ASCE/SEI 41-23,[30] as **Fig. 15** illustrates. The beams and columns were modeled with concentrated plastic hinges; the moment-rotation relationships of the hinge springs for the beam and column components were assigned using their flexural capacities. The plastic hinges represent the inelastic flexural response of the components. Component effective

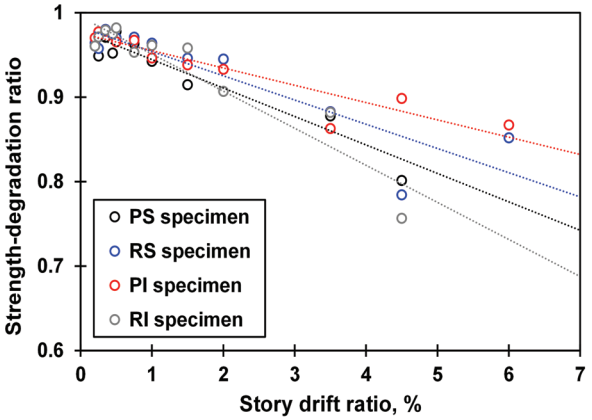

Strength ratio in second loading cycle α_2

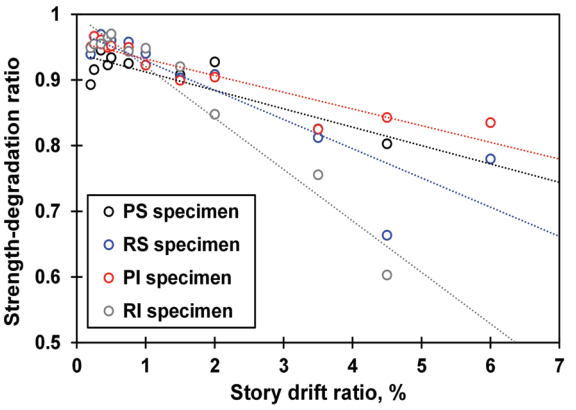

Strength ratio in the third loading cycle α_3

Figure 14. Cyclic strength degradation of test specimens. Note: PI = precast concrete intermediate moment frame system; PS = precast concrete special moment frame system; RI = cast-in-place concrete intermediate moment frame system with monolithic connection details; RS = cast-in-place concrete special moment frame system with monolithic connection details.

Table 5. Evaluation of test specimens based on ACI 374.1 criteria

Criteria		PS	RS	PI	RI
ACI 374.1 9.1.1	Q_n, kN	246.2 (-246.2)	248.6 (-248.6)	214.7 (-214.7)	212.0 (-212.0)
	θ_n, %	0.70 (-0.84)	0.69 (-1.24)	1.47 (-1.46)	0.87 (-0.97)
	θ_{limit}, %	0.40	0.40	0.49	0.49
ACI 374.1 9.1.2	Q_{max}, kN	277.4 (-257.2)	272.6 (-257.0)	241.0 (-234.2)	219.6 (-218.6)
	λQ_n, kN	456.8 (-456.8)	442.0 (-442.0)	336.0 (-336.0)	321.8 (-321.8)
ACI 374.1 9.1.3(1)	$Q_{3.5\%\ 3rd\ cycle}$, kN	239.4 (-196.6)	216.2 (-206.2)	189.8 (-202.2)	158.2 (-155.2)
	$0.75Q_{max}$, kN	208.1 (-192.9)	204.5 (-192.8)	180.8 (-175.7)	164.7 (-164.0)
ACI 374.1 9.1.3(2)	$E_{i.3.5\%\ 3rd\ cycle}$, kN-m*	33.0	22.7	12.9	19.6
	$E_{t.3.5\%\ 3rd\ cycle}$, kN-m†	96.5	93.2	87.2	69.6
	β	34.0	24.3	14.8	28.1
ACI 374.1 9.1.3(3)	$K_{s.3.5\%\ 3rd\ cycle}$, kN/mm‡	1.50 (1.16)	1.30 (1.31)	0.42 (0.46)	0.32 (0.34)
	$0.05K_i$, kN/mm§	0.94 (0.88)	1.10 (0.95)	0.87 (0.76)	0.88 (0.77)

* Dissipated energy during the third cycle at 3.5% drift ratio.

† Idealized energy, calculated as the area of the circumscribing parallelograms defined by the initial stiffness and the peak lateral resistances in positive and negative directions.

‡ Secant stiffness from a drift ratio of –0.35% to a drift ratio of 0.35%.

§ Initial stiffness of test specimens.

Note: Numbers in parenthesis denote negative direction values. $E_{i.3.5\%\ 3rd\ cycle}$ = dissipated energy during the third cycle at 3.5% drift ratio; $E_{t.3.5\%\ 3rd\ cycle}$ = idealized energy, calculated as the area of the circumscribing parallelograms defined by the initial stiffness and the peak lateral resistances in positive and negative directions; K_i = initial stiffness of test specimens; $K_{s.3.5\%\ 3rd\ cycle}$ = secant stiffness from a drift ratio of –0.35% to a drift ratio of 0.35%; PI = precast concrete intermediate moment frame system; PS = precast concrete special moment frame system; Q_{max} = test peak load of specimen; Q_n = nominal lateral-load capacity of specimen; $Q_{3.5\%\ 3rd\ cycle}$ = test load at a 3.5% drift ratio; RI = cast-in-place concrete intermediate moment frame system with monolithic connection details; RS = cast-in-place concrete special moment frame system with monolithic connection details; β = relative energy dissipation ratio; λ = beam–column strength ratio of test specimen; θ_{limit} = drift ratio limit consistent with the *International Building Code* allowable story drift limitation; θ_n = story drift ratio at which the test load reached the nominal strength. 1 mm = 0.039 in.; 1 kN = 0.225 kip; 1 kN-m = 0.738 kip-ft.

stiffnesses in the linear-elastic range were computed following section 10.3 of ASCE/SEI 41. For nonprestressed beams and columns with an axial-load ratio not exceeding 0.1, the effective flexural stiffnesses were taken as $0.3E_{cE}I_b$ and $0.3E_{cE}I_c$, respectively, where E_{cE} is the elastic modulus of concrete, and I_b and I_c are the moment of inertia of the beam and column about the centroidal axis, respectively. Because the tests were conducted under an axial-load ratio of 0.10, the effective stiffness values $0.3EI$ were used to maintain consistency between the experimental conditions and the analytical assumptions.

ASCE/SEI 41[30] presents two distinct strategies in nonlinear modeling for beam–column joints. In both approaches, plastic-hinge properties are assigned to the beam and column elements adjoining the joint interface. The first method is an explicit joint model in which the beams and columns are connected by rigid elements while the joint is represented by a shear-deformation spring that captures the effect of shear distortion on joint performance. The second approach is an implicit joint model in which rigid elements are introduced only for selected components depending on the beam-to-column flexural strength ratio. In this study, because the column flexural strengths exceeded the beam flexural strengths in all test specimens, the columns and beams were connected through rigid elements (Fig. 15). The rigid elements represent rigid end zones at the component–joint interface.

A concentrated plastic-hinge formulation was combined with an explicit joint model to construct the macromodel of the beam–column connection. Nonlinear analyses were performed using the OpenSees platform.

Because the plastic rotation limits in ASCE/SEI 41[30] are generally conservative for displacement capacity,[31–32] the modified Ibarra-Medina-Krawinkler deterioration model[33] was adopted for the beam hinge elements to simulate the hysteretic behavior of both precast and cast-in-place concrete specimens. **Table 6** summarizes the modeling parameters. In the explicit joint model, a zero-length rotational spring was added at the joint to represent panel zone shear deformation, and its elastic rotational stiffness of joint $k_{e,j}$ was calibrated using the test results to match the elastic rotational stiffness of the joint; thus the model reproduces the measured elastic response prior

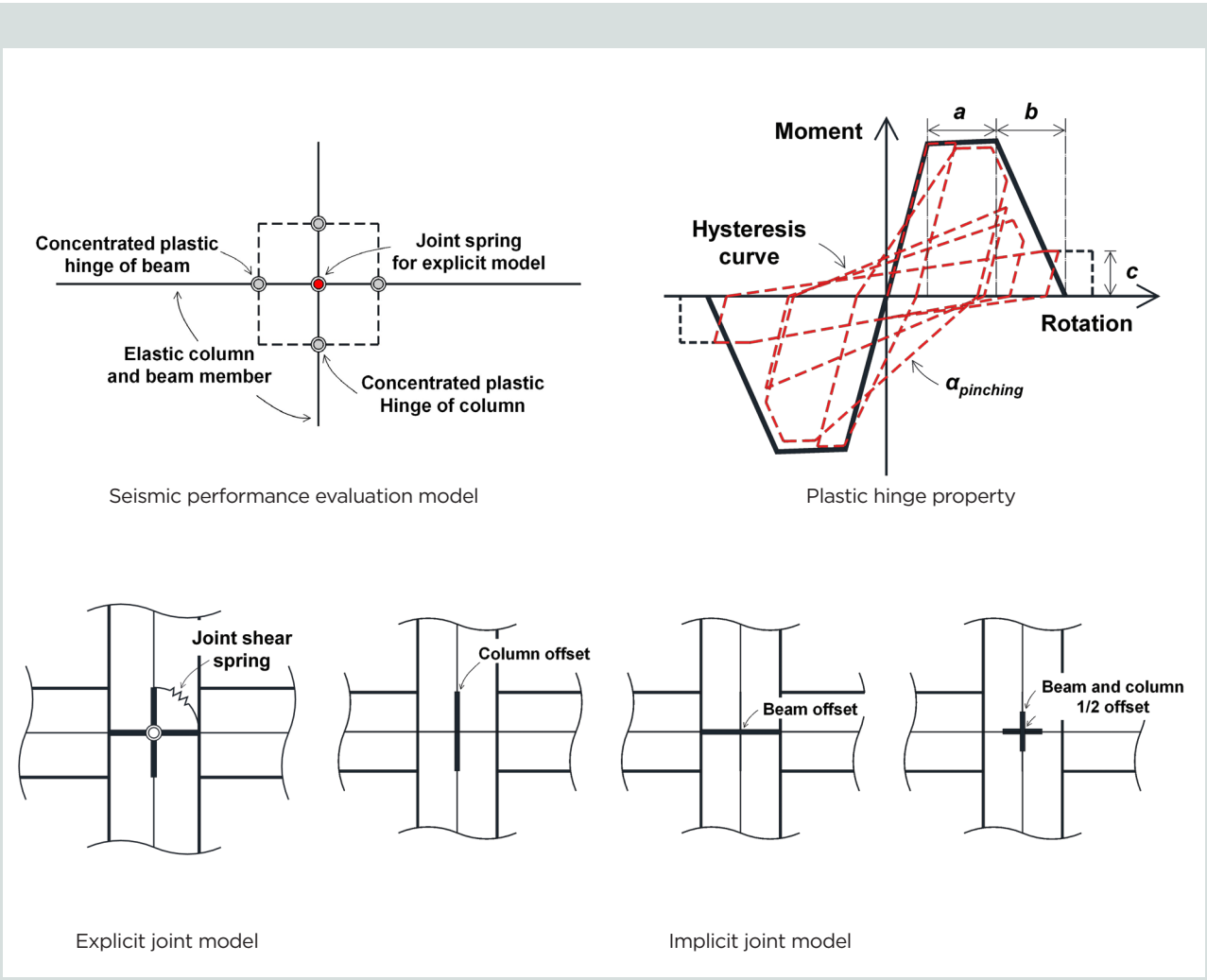

Figure 15. American Society of Civil Engineers/Structural Engineering Institute's *Seismic Evaluation and Retrofit of Existing Buildings*, ASCE/SEI 41-23, beam–column joint modeling. Note: *a* = plastic plateau; *b* = plastic range; *c* = residual strength ratio; $\alpha_{pinching}$ = ratio of the force at which reloading begins.

Table 6. Modeling parameters

Specimen		$M_{y,b}$, kN-m	$k_{e,b}$, kN-m/radian	$k_{e,c}$, kN-m/radian	$k_{e,j}$, kN-m/radian	*a*, radians	*b*, radians	*c*	$\alpha_{pinching}$
SMF	PS	341.2	1.54×10^5	1.80×10^5	1.37×10^6	0.035	0.27	0.6	0.6
	RS	367.8	1.54×10^5	1.80×10^5	1.05×10^6	0.04	0.26	0.6	0.3
IMF	PI	297.6	1.54×10^5	1.80×10^5	1.63×10^6	0.025	0.27	0.6	0.3
	RI	296.5	1.54×10^5	1.80×10^5	1.22×10^6	0.03	0.27	0.6	0.6

Note: *a* = plastic plateau; *b* = plastic range; *c* = residual strength ratio; IMF = intermediate moment frame; $k_{e,b}$ = rotational stiffness of beam hinge spring; $k_{e,c}$ = rotational stiffness of column hinge spring; $k_{e,j}$ = rotational stiffness of joint spring; $M_{y,b}$ = beam yield flexural strength; SMF = special moment frame; $\alpha_{pinching}$ = ratio of the force at which reloading begins. rad. = radians; 1 kN-m = 0.738 kip-ft.

to significant cracking and yielding. The joint spring represents joint-panel shear deformation and was calibrated using the test response.

Figure 16 compares the experimental hysteresis curves with the analytical cyclic responses. The analyses reflected the stiffness degradation, ductile behavior, and energy dissipation characteristics under cyclic loading with reasonable analytical accuracy; in particular, the peak and residual strengths matched the test results closely. For some specimens, the analyses also simulated pinching behavior and cyclic strength loss to a practical extent. Based on these results, the analytical model

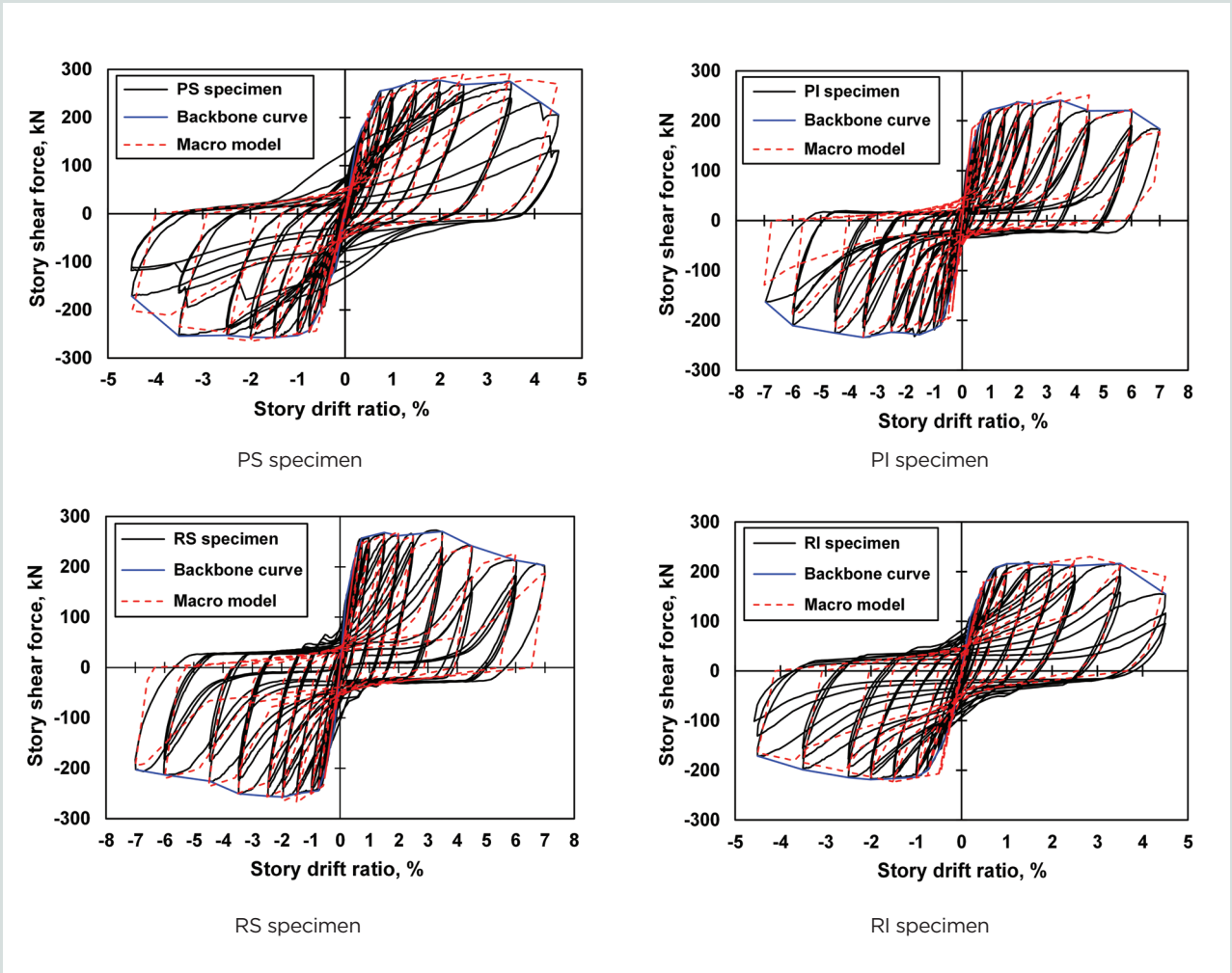

Figure 16. Comparison of experimental and analytical results for the test specimens. Note: PI = precast concrete intermediate moment frame system; PS = precast concrete special moment frame system; RI = cast-in-place concrete intermediate moment frame system with monolithic connection details; RS = cast-in-place concrete special moment frame system with monolithic connection details. 1 kN = 0.225 kip.

constructed using the modeling parameters in Table 6 showed good agreement with the cyclic responses of both the cast-in-place and precast concrete specimen series. Accordingly, the proposed model is expected to provide a quick practical method for performance-based seismic design and seismic performance evaluation of precast concrete dry joint details.

Conclusion

In this study, specimens detailed for special and intermediate moment frames were fabricated to propose a self-sustaining dry precast concrete beam–column connection system. The performance of these specimens was compared with conventional (wet splicing) reinforced concrete specimens through both experiments and analyses. The experimental results were quantified, and the seismic performance of the specimens was evaluated analytically by macromodeling using an explicit joint model. The results of the experiments, analyses, and modeling support the following conclusions:

- By using innovative dry mechanical splices, the proposed self-sustaining precast concrete system can provide good stability during erection and site assembly stages without temporary shoring. Also, it can improve constructibility of multistory precast concrete moment frame systems.
- Precast concrete specimens with special and intermediate seismic details exhibited ductile hysteresis responses comparable to those of the cast-in-place specimens in terms of strength, displacement capacity, and failure mode. Flexural failure was observed at the designated locations of beam components, which is consistent with the strong column–weak beam philosophy. In the PS specimen, fracture of the longitudinal reinforcement occurred outside of the mechanical splice region, confirming adequate safety within the joint panel zone.
- The strain response of the longitudinal reinforcement in the precast concrete beams indicates that the mechanical

splices performed adequately. In the PS specimen, which was detailed as a strong connection, yielding was intentionally forced to occur outside the splice region, and no bar yielding was observed within the joint core, demonstrating behavior appropriate for special moment frame connections constructed using precast concrete.

- The dry precast concrete connections achieved seismic performance comparable to monolithic cast-in-place connections with respect to ductility, energy dissipation capacity (including equivalent viscous damping behavior), and strength degradation. These results support the practical application of the proposed mechanical splices to the emulative precast concrete systems.

- The proposed macromodel, combining concentrated plastic hinges with an explicit joint rotational spring, reproduced the key cyclic response characteristics (stiffness degradation, pinching, and strength loss). Peak and residual strengths were captured with good agreement, indicating that the approach can be used for comparative assessment of joint details and performance-based evaluation.

Acknowledgments

This work was supported by the National Research Foundation of Korea grant RS-2023-00209647, funded by the Korean government's Ministry of Science and ICT.

References

1. Han, S. J., M. S. Kim, I. Heo, W. J. Lee, and D. Lee. 2025. "Performances of Precast Concrete Composite Double Wall Systems with Discontinuous Steel Members as Shear Connector." *Steel and Composite Structures* 55 (4): 283–295. https://doi.org/10.12989/scs.2025.55.4.283.

2. Zhang, W., D. Lee, S. H. Kim, H. J. Ju, and C. J. Lee, C. J. 2023. "Seismic Performance of Precast Wide Beam-Column Connections with Asymmetrical Anchorage Reinforcement Details." *Engineering Structures*, no. 275, 115237. https://doi.org/10.1016/j.engstruct.2022.115237.

3. Lee, J. D., J. K. Yoon, and T. H.-K. Kang. 2016. "Combined Half Precast Concrete Slab and Post-tensioned Slab Topping System for Basement Parking Structures." *Journal of Structural Integrity and Maintenance* 1 (1): 1–9. https://doi.org/10.1080/24705314.2016.1153281.

4. Kim, J. H., B. S. Jang, S. H. Choi, Y. J. Lee, H. S. Jeong, and K. S. Kim. 2021. "Experimental Study on Lateral Behavior of Precast Wide Beam-Column Joints." *Earthquakes and Structures* 21 (6): 653–667. https://doi.org/10.12989/eas.2021.21.6.653.

5. Memon, S. A., M. Zain, D. Zhang, S. K. U. Rehman, M. Usman, and D. Lee. 2020. "Emerging Trends in the Growth of Structural Systems for Tall Buildings." *Journal of Structural Integrity and Maintenance* 5 (3): 155–170. https://doi.org/10.1080/24705314.2020.1765270.

6. Kim, S. H., T. H.-K. Kang, D. J. Jung, and J. M. LaFave. 2021. "Seismic Behavior of Precast and Post-tensioned Exterior Connections with Ductile Headed Rods." *ACI Structural Journal* 118 (1): 87–100. https://doi.org/10.14359/51728179.

7. Lee, D., T. H.-K. Kang, H. Ju, S. W. Moon, and I. S. Yang, I. S. 2019. "Seismic Performance of RC Column-Foundation Connections with Combo-Type Mechanical Splices." *ACI Structural Journal* 116 (5): 173–186. https://doi.org/10.14359/51716766.

8. Haber, Z. B., M. S. Saiidi, and D. H. Sanders. 2014. "Seismic Performance of Precast Columns with Mechanically Spliced Column-Footing Connections." *ACI Structural Journal* 111 (3): 639–650. https://doi.org/10.14359/51686624.

9. Chun, S. C., Baek, J. W., Kang, T. H.-K., and Kim, M. G. 2020. "Cyclic Loading Tests of Slab-Wall Connections Using Removable Rail Mechanical Splices." *ACI Structural Journal* 117 (3): 155–167. https://doi.org/10.14359/51723505.

10. Kim, S. H., D. Lee, Y. K. Kim, S. W. Lee, U. Y. Yeo, and J. E. Park. 2023. "Seismic Performance Evaluation of Dry Precast Concrete Beam-Column Connections with Special Moment Frame Details." [In Korean.] *EESK Journal of Earthquake Engineering* 27 (5): 203–211. https://doi.org/10.5000/EESK.2023.27.5.203.

11. Kim, S. H., J. Cho, H. K. Oh, S. D. Choi, U. Y. Yeo, and D. Lee. 2023. "Seismic Performance Evaluation of Dry Precast Concrete Beam-Column Connections with Intermediate Moment Frame Details." [In Korean.] *EESK Journal of Earthquake Engineering* 27 (3): 129–137. https://doi.org/10.5000/EESK.2023.27.3.129.

12. Lee, D. 2025. "Innovative PC Dry Mechanical Splice." YouTube playlist. https://www.youtube.com/playlist?list=PLlWogJfdwIaeBDt-lGGAtYOioYE69v8O1.

13. ACI (American Concrete Institute) Committee 318. 2025. *Building Code for Structural Concrete—Code Requirements and Commentary*. ACI CODE-318-25. Farmington Hills, MI: ACI.

14. Joint ACI/PCI Committee 319. 2025. *Structural Precast Concrete—Code Requirements and Commentary*. ACI/PCI 319-25. Farmington Hills, MI: ACI; Chicago, IL: PCI.

15. Zhang, W., S. H. Kim, D. Lee, H. J. Ju, L. Dai, and L. Wang. 2025. "Seismic Performance of Innovative Precast Dry and Strong Beam-Column Connection." *Journal of Building Engineering*, no. 106, 112711. https://doi.org/10.1016/j.jobe.2025.112711.

16. KATS (Korean Agency for Technology and Standards). 2024. *Method of Inspection for Mechanical Splicing Joint of Bars for Concrete Reinforcement*. KS D 0249. [In Korean.] Sejong, Republic of Korea: KATS.

17. ACI Committee 374. 2005. *Acceptance Criteria for Moment Frames Based on Structural Testing and Commentary*. ACI 374.1-05(19). Farmington Hills, MI: ACI.

18. ACI Committee 352. 2002. *Recommendations for Design of Beam-Column Connections in Monolithic Reinforced Concrete Structures*. ACI 352R-02. Farmington Hills, MI: ACI.

19. Zhang, W., S. H. Kim, and D. H. Lee. 2023. "Seismic Performance of Self-sustaining Precast Wide Beam-Column Connections for Fast-Built Construction." *Computers and Concrete* 32 (3): 339–349. https://doi.org/10.12989/cac.2023.32.3.339.

20. Alawad, O. M., M. J. Gombeda, C. J. Naito, and S. E. Quiel. 2019. "Simplified Methodologies for Preliminary Blast-Resistant Design of Precast Concrete Wall Panels." *PCI Journal* 64 (4): 55–70. https://doi.org/10.15554/pcij64.4-03.

21. Requena-Garcia-Cruz, M. V., A. Morales-Esteban, P. Durand-Neyra, and B. Zapico-Blanco. 2021. "Influence of the Constructive Features of RC Existing Buildings in Their Ductility and Seismic Performance." *Bulletin of Earthquake Engineering* 19 (1): 377–401. https://doi.org/10.1007/s10518-020-00984-z.

22. Eom, T. S., H. G. Park, H. J. Hwang, and S. M. Kang. 2016. "Plastic Hinge Relocation Methods for Emulative PC Beam–Column Connections." *Journal of Structural Engineering* 142 (2): 04015111. https://doi.org/10.1061/(ASCE)ST.1943-541X.0001378.

23. Zhang, W., D. Lee, S. H. Kim, and D. Zhang. 2025. "Seismic Performance of Precast Concrete Wide Beam-Column Connections under Ductile Connection Principle." *ACI Structural Journal* 122 (2): 201–214. https://doi.org/10.14359/51744399.

24. Feng, F., K. Jiang, H. J. Hwang, and W. J. Yi. 2018. "Earthquake Response of Low-Rise RC Moment Frame Structures according to Energy Dissipation Ratio of Beam-Column Joints." *Journal of Structural Integrity and Maintenance* 3 (1): 33–43. https://doi.org/10.1080/24705314.2018.1426171.

25. Zhang, W., D. Lee, W. J. Lee, M. S. Kim, and J. Y. Park. 2023. "Effect of Cast-in-Place Beams on Seismic Performance of Precast Shear Walls." *ACI Structural Journal* 120 (1): 89–102. https://doi.org/10.14359/51737231.

26. Kim, J. H., D. Lee, S. H. Choi, H. Jeong, and K. S. Kim. 2022. "Seismic Performance of Precast Multi-span Frame System Integrated by Unbonded Tendons." *ACI Structural Journal* 119 (5): 193–206. https://doi.org/10.14359/51734801.

27. Chang, H. J., I. Choi, J. H. Kim, and S. Y. Hong. 2021. "Experimental Investigation on Seismic Performance of Two Types of Member-Panel Zone Unified Joints for Precast Concrete Moment-Resisting Frame." *Journal of Building Engineering*, no. 43, 103202. https://doi.org/10.1016/j.jobe.2021.103202.

28. Guan, D., R. Xu, S. Yang, Z. Chen, and Z. Guo. 2022. "Development and Seismic Behavior of a Novel UHPC-Shell Strengthened Prefabricated Concrete Column." *Journal of Building Engineering*, no. 46, 103672. https://doi.org/10.1016/j.jobe.2021.103672.

29. Guan, D., C. Jiang, Z. Guo, and H. Ge. 2018. "Development and Seismic Behavior of Precast Concrete Beam-to-Column Connections." *Journal of Earthquake Engineering* 22 (2): 234–256. https://doi.org/10.1080/13632469.2016.1217807.

30. ASCE/SEI (Structural Engineering Institute). 2023. *Seismic Evaluation and Retrofit of Existing Buildings*. ASCE/SEI 41-23. Reston, VA: American Society of Civil Engineers. https://doi.org/10.1061/9780784416112.

31. Eom, T. S., H. J. Hwang, and H. G. Park. 2015. "Energy-Based Hysteresis Model for Reinforced Concrete Beam-Column Connections." *ACI Structural Journal* 112 (2): 157–166. https://doi.org/10.14359/51687404.

32. Hwang, H. J., and H. G. Park. 2021. "Plastic Hinge Model for Performance-Based Design of Beam-Column Joints." *Journal of Structural Engineering* 147 (2): 04020336. https://doi.org/10.1061/(ASCE)ST.1943-541X.0002892.

33. Ibarra, L. F., R. A. Medina, and H. Krawinkler. 2005. "Hysteretic Models that Incorporate Strength and Stiffness Deterioration." *Earthquake Engineering and Structural Dynamics* 34 (12): 1489–1511. https://doi.org/10.1002/eqe.495.

Notation

a = plastic plateau

A_{s1} = total cross-sectional areas of the tension reinforcement in left beam

A_{s2} = total cross-sectional areas of the tension reinforcement in right beam

b = plastic range

b_j = the effective width of the joint transverse to the direction of shear

c = residual strength ratio

E_{cE} = elastic modulus of concrete

$E_{i.3.5\%\ 3rd\ cycle}$ = dissipated energy during the third cycle at 3.5% drift ratio

E_I = dissipated energy of a target hysteresis loop

E_{so} = static strain energy for linear-elastic response

$E_{t.3.5\%\ 3rd\ cycle}$ = idealized energy, calculated as the area of the circumscribing parallelograms defined by the initial stiffness and the peak lateral resistances in positive and negative directions

EI = flexural rigidity of the component

f'_c = compressive strength of concrete

f'_g = compressive strength of grout

$f_{u.test}$ = tensile strength of the reinforcement measured from tensile test

f_y = specified yield strength of nonprestressed reinforcement

$f_{y.test}$ = yield strength of the reinforcement measured from tensile test

h_b = depth of beam

h_c = depth of column

h_{co} = bracket depth

h_{eff} = effective column height

i = cycle number at a given drift level

I_b = the moment of inertia of the beam gross section about the centroidal axis

I_c = the moment of inertia of the column gross section about the centroidal axis

j = drift level

$k_{e,b}$ = elastic rotation stiffness of beam hinge spring

$k_{e,c}$ = elastic rotation stiffness of column hinge spring

$k_{e,j}$ = elastic rotational stiffness of joint hinge spring

K_I = initial stiffness of test specimens

$K_{s.3.5\%\ 3rd\ cycle}$ = secant stiffness from a drift ratio of -0.35% to a drift ratio of 0.35%

l_b = single beam span length

l_{sp} = mechanical coupler length

L_b = beam span length

L_{sp} = length of mechanical splice

$M_{n,b}$ = nominal flexural strength of beam section

$M^+_{n,b}$ = nominal positive flexural strength of beam section

$M^-_{n,b}$ = nominal negative flexural strength of beam section

$M_{n,c}$ = nominal flexural strength of column section

$M_{pr,b}$ = probable flexural strength of beam (determined using the properties of the beam at joint faces assuming a tensile stress in longitudinal reinforcement of at least $1.25f_y$)

M_u = factored flexural moment of beam

$M_{y,b}$ = beam yield flexural strength

$Q^j_{1,max}$ = average peak load of the positive and negative directions in the *i*th cycle at the *j*th drift level

Q_{max} = test peak load of specimen

Q_n = nominal lateral-load capacity of specimen

$Q_{n.PC}$ = nominal lateral-load capacity of precast concrete specimen considering bracket depth and seating length of precast concrete beam

$Q_{n.RC}$ = nominal lateral-load capacity of cast-in-place concrete specimen

Q_y = yield load of test specimen

$Q^j_{i,max}$ = average peak load of the positive and negative directions in the first cycle at the *j*th drift level

$Q_{3.5\%\ 3rd\ cycle}$ = test load at a 3.5% drift ratio

s = seating length of precast concrete beam

$S_{e,b}$ = probable flexural strength (moment at connection corresponding to development of probable strength intended yield locations, based on the governing mechanism of inelastic lateral deformation)

T_1 = maximum tensile force in the tension reinforcement of left beam

T_2 = maximum tensile force in the tension reinforcement of right beam

V_{jh} = maximum joint shear force

V_{jn} = joint shear strength

α = stress multiplier that accounts for the increased flexural strength due to strain hardening and is typically taken as 1.25 for special moment frames

α_i = strength degradation for each specimen evaluated by addressing the strength-degradation ratio in *i*th loading cycle

$\alpha_{pinching}$ = ratio of the force at which reloading begins

α_2 = strength degradation for each specimen evaluated using the strength-degradation ratio in the second cycle

α_3 = strength degradation for each specimen evaluated using the strength-degradation ratio in the third cycle

β = relative energy dissipation ratio

γ = coefficient addressing the confinement effect of the beams framed into the joint based on the specimen geometry

δ_r = residual displacement of mechanical splice

ε_y = yield strain

θ = rotation

θ_{limit} = drift ratio limit consistent with the *International Building Code* allowable story drift limitation

θ_{max} = story drift ratio at peak load

θ_n = story drift ratio at which the test load reached the nominal strength

θ_u = drift ratio at ultimate displacement

θ_y = story drift ratio at yield load

λ = beam–column strength ratio of test specimen

μ = ductility capacity of test specimen

$\mu\varepsilon$ = strain of reinforcement

ξ_{eq} = equivalent viscous damping ratio

ϕ = strength reduction factor

$\phi M_{n,j}$ = design flexural strength of strong connection

About the authors

Seon-Hoon Kim is a PhD student in the Department of Global Smart City at Sungkyunkwan University (SKKU) in Suwon, Korea.

Deuckhang "DK" Lee, PhD, is an associate professor in the School of Civil, Architectural Engineering, and Landscape Architecture and the Department of Global Smart City at SKKU.

Wei Zhang is an assistant professor in the College of Civil and Architectural Engineering at North China University of Science and Technology in Beijing.

Jae-Hyun Kim is a postdoctoral researcher in the College of Civil Engineering at Changsha University of Science and Technology in Changsha, China.

Abstract

This study presents an innovative mechanical splice system to facilitate dry connections for code-compliant precast concrete beam–column joints. To evaluate its emulative seismic performance, two precast concrete beam–column subassembly specimens were designed and fabricated in accordance with seismic design provisions for special and intermediate moment frames. They were tested under cyclic loading, with two conventional cast-in-place control specimens. The precast concrete specimens with dry mechanical splices exhibited strength, ductility, failure modes, strain responses, energy dissipation, and strength degradation characteristics comparable with those of the control specimens under the test conditions. This demonstrates that the proposed seismic details can achieve emulative seismic performance. Researchers developed a lumped-plastic-hinge analysis model with an explicit joint element to simulate, using nonlinear conditions, the performance of precast concrete moment frame systems with dry connections. The model's analytical hysteretic responses agreed with the measured cyclic behavior of the physical specimens, confirming the applicability of the model proposed for precast concrete beam–column connections.

Keywords

Beam–column connections, dry joint, emulative detailing, mechanical splice, precast concrete, strong connection.

Review policy

This paper was reviewed in accordance with the Precast/Prestressed Concrete Institute's peer-review process. The Precast/Prestressed Concrete Institute is not responsible for statements made by authors of papers in *PCI Journal*. No payment is offered.

Publishing details

This paper appears in *PCI Journal* (ISSN 0887-9672) V. 71, No. 4, July–August 2026, and can be found at https://doi.org/10.15554/pcij71.4-02. *PCI Journal* is published bimonthly by the Precast/Prestressed Concrete Institute, 8770 W. Bryn Mawr Ave., Suite 1150, Chicago, IL 60631.

Reader comments

Please address any reader comments to journal@pci.org or Precast/Prestressed Concrete Institute, c/o *PCI Journal*, 8770 W. Bryn Mawr Ave., Suite 1150, Chicago, IL 60631.